



Impact of gold and silver nanoparticles injected in blood with viscous dissipation

Haris Alam Zuberi^a, Madan Lal^a, Shivangi Verma^a, Ali J. Chamkha^{b*} and Nurul Amira Zainal^{c#}

^aDepartment of Applied Mathematics, M. J. P. Rohilkhand University, Bareilly, India; ^bFaculty of Engineering, Kuwait College of Science and Technology, Doha District, Kuwait; ^cFakulti Teknologi dan Kejuruteraan Mekanikal, Universiti Teknikal Malaysia Melaka, Hang Tuah Jaya, 76100 Durian Tunggal, Melaka, Malaysia

ABSTRACT

A nano-blood model is developed to study the flow of gold- and silver-infused blood through a porous, stenotic artery under Newtonian assumptions. Wall curvature, convective heating, wall motion, and viscous dissipation are considered. Darcy's model simulates porous resistance, and the Tiwari-Das model captures nanoparticle effects. Governing equations are reduced via similarity transformations and solved using MATLAB's bvp4c solver. Validation against existing studies is provided. Results show gold-blood nanofluid achieves higher velocities than silver-blood. Increasing the Biot number enhances cooling at the arterial wall. Detailed graphs and 3D contour plots illustrate the effects on temperature, velocity, skin friction, and Nusselt number.

ARTICLE HISTORY

Received 25 January 2024 Accepted 13 April 2025

KEYWORDS

Blood; nanofluid; gold and silver nanoparticles; MHD; bvp4c; MATLAB

1. Introduction

Blood flow plays a crucial role in removing metabolic waste products from cells. Blood carries oxygen and essential nutrients to every cell in the body. When blood flow is compromised, cells may not receive an adequate supply of these vital elements, which can lead to cell dysfunction or even cell death. A magnetic field is known to impact the flow of blood significantly (Tzirtzilakis 2005). Certain studies propose the possibility of employing external magnetic fields to exert control or manipulate blood flow under particular circumstances. For example, certain experiments have explored the possibility of using magnetic fields to guide or steer magnetic nanoparticles in the bloodstream to targeted areas for medical purposes, such as drug delivery or tumor treatment. In a stenotic artery, blood flow is hindered due to the narrowing of the artery caused by plaque buildup or other factors. The reduced diameter of the artery restricts the normal flow of blood, which can lead to various consequences depending on the location and severity of the stenosis (Abumandour et al. 2022). When blood flow is impeded in a stenotic artery, the narrowed artery limits the amount of oxygen and nutrients that can reach the tissues and organs downstream from the stenosis. This can lead to ischemia, a condition where cells do not receive sufficient oxygen and nutrients to function properly. The narrowed space in the stenotic artery may cause turbulence in the blood flow, leading to platelet activation and clot formation (Alhussain 2022). These blood clots can partially or completely block the artery, further impeding blood flow. If the stenotic artery is part of the coronary arteries supplying the heart muscle, reduced blood flow can lead to decreased oxygen supply to it. This places additional strain on the heart, leading to symptoms like chest pain (angina) or, in severe cases, a heart attack (myocardial infarction) (Ashwini et al. 2022). Depending on the location of the stenotic artery, various organs supplied by that artery can be affected. For example, stenosis in the carotid artery can increase the risk of stroke, while stenosis in the peripheral arteries can lead to pain, numbness, or tissue damage in the affected limbs. In some cases, the plaque within the stenotic artery can become unstable and rupture, triggering the formation of a blood clot. If the clot completely blocks the artery, it can result in severe consequences such as heart attack, stroke, or limbthreatening ischemia (Das et al. 2022). The management of blood flow in a stenotic artery depends on the specific situation and severity. Treatment may involve lifestyle changes (e.g. adopting a heart-healthy

diet and regular exercise), medications to manage risk factors (e.g. statins to lower cholesterol or antiplatelet drugs to prevent clot formation), and interventions such as angioplasty and stent placement to widen the narrowed artery. In severe cases, bypass surgery may be required to reroute blood flow around the stenotic segment. Early detection and appropriate management of stenotic arteries are crucial to prevent complications and improve overall cardiovascular health (Sarwar et al. 2022; Fangfang et al. 2023).

Nanotechnology has emerged as a transformative force in the realm of fluid dynamics, offering unprecedented opportunities for advancing biomedical interventions. Nanostructured materials, particularly nanoparticles, play a pivotal role in the treatment of various biomedical conditions, including stenosis (Cheng et al. 2008; King and Gee 2010). These nanoparticles, owing to their unique physicochemical properties, can be tailored to interact with biological systems at the nanoscale, thereby enabling precise targeting and delivery of therapeutic agents to diseased tissues. The nanoparticle-based drug delivery systems offer a promising avenue for mitigating the progression of arterial narrowing and reducing associated complications. The encapsulation of therapeutic agents within nanoparticles allows researchers to enhance drug stability, improve bioavailability, and achieve targeted delivery to the site of stenotic lesions (Vedernikova 2015). Furthermore, nanotechnology facilitates the development of innovative diagnostic tools and imaging agents for early detection and monitoring of stenotic lesions, enabling timely intervention and personalized treatment strategies. Overall, the integration of nanotechnology into fluid dynamics holds immense potential for revolutionizing the diagnosis, treatment, and management of various biomedical conditions, including stenosis, thereby significantly improving patient outcomes and quality of life.

The size and shape of the nanoparticles play a crucial role in determining their behavior. Smaller nanoparticles are more likely to follow the flow of blood and pass through narrow spaces, while larger nanoparticles may get trapped or interact with the endothelial lining of the artery (Khanduri et al. 2023). Blood flow in a stenotic artery can be complex, with regions of high velocity and turbulence near the stenosis. The behavior of nanoparticles can be influenced by these flow conditions, affecting their distribution and residence time. Gold and silver nanoparticles have surface properties that promote adhesion to the endothelial lining or interaction with blood cells. In

regions of disturbed flow or damaged endothelium, nanoparticles may accumulate or interact differently compared to normal blood flow conditions (Elhanafy et al. 2023). The trajectory of nanoparticles in blood flow under a stenotic artery can be influenced by several factors, including the size, shape, surface properties of the nanoparticles, blood flow conditions, and the degree of stenosis. As with other nanoparticles, one important field of research concerns how gold and silver nanoparticles behave in the bloodstream, particularly for applications such as targeted drug delivery and medical imaging (Khanduri and Sharma 2023). In recent years, there has been a growing interest in the study of thermal engineering, particularly in the context of solving complex real-world problems. The work by Rehman, Trabelsi, et al. (2023) provides valuable contributions to this field, offering in-depth analyses and solutions to a range of thermal engineering problems. Their findings serve as a cornerstone for understanding the intricate dynamics of heat transfer, fluid flow, and energy conversion processes, which are essential for addressing contemporary challenges in engineering and technology. Further, the exploration by Rehman, Alfaleh, et al. (2023) is enriched by a thorough review of relevant literature, which underscores the significance of phenomena such as Casson nanoliquid flow, Darcy-Forchheimer and the traditional Jeffery-Hamel flow. Furthermore, the incorporation of influential theories such as the Cattaneo-Christov heat flux theory adds depth to their analysis, providing valuable insights into the complex interplay of factors including Brownian motion, thermophoretic diffusion, and chemical reactions.

Due to the complexity of blood flow and nanoparticle behavior, researchers use various experimental and computational methods to study nanoparticle dynamics in the presence of a stenotic artery. These include in vitro studies, animal models, and computational fluid dynamics (CFD) simulations (Sajid, Jamshed, et al. 2023). By gaining a better understanding of nanoparticle behavior in stenotic arteries, researchers aim to develop improved nanoparticlebased therapies and diagnostic approaches for cardiovascular diseases. It is important to note that while nanoparticles hold promising potential for medical applications, their use in patients requires thorough safety and efficacy evaluations through preclinical and clinical studies. Boujelbene et al. (2023) delved into the intricate dynamics of Carreau iron oxide blood nanofluid traversing narrower arteries. They developed a comprehensive model that not only sheds light on the fundamental mechanisms governing nanodrug delivery but also holds significant implications for advancing cancer treatment strategies. The study highlights the critical discussion surrounding irreversibility phenomena inherent in drug delivery processes, emphasizing the necessity to meticulously consider the dosage of nanoparticles employed, particularly in cancer treatment modalities reliant on melting heating. Moreover, the elucidation of temperature elevation as a function of viscous dissipation and thermal radiation underscores the multifaceted nature of this complex phenomenon, paving the way for innovative approaches in biomedical engineering and therapeutic interventions. The combined impacts of Cattaneo-Christove (C-C) heat flux provide valuable insights into entropy production and energy dissipation in engineering applications as investigated by Khedher et al. (2023).

Several researches have been carried out on different types of nanoparticles for different systems. Sarwar and Hussain (2021) discussed the gold nanoparticles in a stenotic artery. Aarathy et al. (2020) investigated the structures of various magnetic nanoparticles for hyperthermia. Liu et al. (2012) examined the shape factor of nanoparticles for a better drug delivery system. Xamada-Ota and Xue's models have been analyzed for microchannel by Alharbi et al. (2024). Zheng (2014) discussed the simulation of nanoparticle transportation in pulmonary vessels. Hybrid nanofluids allow for the tuning of specific properties to meet the requirements of particular applications. Hybrid nanofluids can be used for drug delivery systems, diagnostics, and imaging (Tripathi, Vasu, Subba Reddy Gorla, et al. 2021; Govindarajulu and Subramanyam Reddy 2022; Thirumalaisamy et al. 2022; Lund et al. 2023). They may also be engineered to have antimicrobial properties. Sajid, Gari, et al. (2023) have explored tetra hybrid binary nanofluid flows via the Riga wedge. Various transport phenomena in a hybrid nanofluid under the influence of magnetohydrodynamics and autocatalytic chemical reactions have been a part of research by Rehman, Alqahtani, et al. (2023). Verma (2018) analyzed and simulated nanofluid flow using MATLAB. Ratha et al. (2023) analyzed the effect of the nanoparticle's shape on stretching cylinder flows. Boujelbene et al. (2025) employed the Keller-Box method to explore the phenomenon of entropy degradation in the context of a dual diffusion flow of non-Newtonian fluids within an inclined channel.

Viscous dissipation in blood flow in a stenotic artery refers to the conversion of mechanical energy into heat due to the resistance encountered by blood as it flows through a narrowed or constricted arterial segment (Abid and Hasnain 2024; Mishra 2024). When an artery becomes stenotic (narrowed), the flow of blood through this narrowed region becomes more turbulent, leading to increased frictional forces between the blood and the vessel wall. This frictional force results in energy loss in the form of heat, which is termed viscous dissipation (Painter et al. 2006). It is an important factor to consider in the study of blood flow dynamics, particularly in situations such as arterial stenosis, where alterations in flow patterns and energy losses can have significant physiological implications. In the context of hemodynamics, understanding viscous dissipation can provide insights into the distribution of blood flow, pressure gradients, and the overall energy expenditure within the cardiovascular system. Computational fluid dynamics (CFD) simulations and mathematical modeling are often employed to quantify the extent of viscous dissipation and its impact on blood flow characteristics in stenotic arteries (Tang et al. 2022). Researchers and clinicians studying cardiovascular diseases, such as atherosclerosis, often investigate the role of viscous dissipation in understanding disease progression, optimizing treatment strategies, and predicting potential complications such as thrombosis or ischemia. Moreover, the stretching and shrinking of the arterial wall, coupled with the presence of porous walls within the artery, play critical roles in shaping the hemodynamic environment and disease progression. Stenosis, characterized by the narrowing of arterial lumens due to plaque buildup or structural changes in the arterial wall, often triggers biomechanical responses that manifest as alterations in arterial geometry. Humphrey (1995) explained that the stretching of the arterial wall occurs as a consequence of increased blood pressure or mechanical stress, leading to outward expansion and dilation of the affected segment. Conversely, the shrinking of the arterial wall may result from pathological changes such as fibrosis or calcification, leading to inward narrowing and constriction of the artery. These dynamic changes in arterial geometry profoundly influence blood flow patterns, pressure distributions, and shear stress profiles within the stenotic region (Omama et al. 2024). Additionally, the presence of porous walls within the artery further complicates the hemodynamic scenario by introducing additional resistance to flow and altering fluid-solid interactions. Porous arterial walls can affect the permeability of the vessel wall, modulate fluid filtration and diffusion processes, and impact

local hemodynamic forces (Fahim et al. 2024). Consequently, understanding the interplay between arterial wall dynamics and porous structures is crucial for elucidating the pathophysiology of stenosis and developing effective diagnostic and therapeutic strategies for this prevalent cardiovascular condition.

Gold and silver nanoparticles (Wagas et al. 2023) are preferred over other nanoparticles for drug targeting in certain applications due to their unique properties, biocompatibility, and ease of surface functionalization. However, it's important to note that the choice of nanoparticles for drug targeting depends on the specific requirements of the application and the intended target site. Different nanoparticles offer distinct advantages and disadvantages, and their selection is tailored to suit the specific needs of the therapeutic or diagnostic approach. Gold and silver nanoparticles have well-established methods for surface functionalization, allowing researchers to easily attach various targeting ligands or drugs to their surfaces (Nicol et al. 2015). This enables targeted drug delivery to specific cells or tissues, enhancing treatment efficacy and reducing side effects. Gold nanoparticles exhibit a unique optical property called surface plasmon resonance, which can be used for imaging and therapeutic purposes. They absorb and scatter light in the visible and near-infrared regions, making them useful for targeted imaging and photothermal therapy (Waqas et al. 2023). Gold and silver nanoparticles are relatively stable and can resist degradation under certain conditions, ensuring that the drugs they carry are protected until they reach the target site. Moreover, Gold and silver nanoparticles can carry a significant amount of drugs due to their large surface area and high drug-loading capacity, making them efficient drug carriers for targeted delivery (Gul et al. 2022; Mashiku and Shaw 2023; Prasad and Bali 2023). Table 1 presents a detailed overview of the thermophysical properties of gold and silver nanoparticles utilized in the treatment of various cardiovascular diseases. This compilation serves as a crucial reference point, shedding light on the distinct characteristics of nanoparticles crucial for therapeutic applications. Hence, gold and silver nanoparticles possess unique physical, chemical, and optical characteristics that enable them for a variety of uses, including the delivery of medications to particular bodily locations (Gomes et al. 2021; Huang et al. 2024; Kalashgrani et al. 2024; Song et al. 2024). Table 2 offers a comprehensive analysis of distinct nanoparticles, encompassing their biocompatibility, potential applications, and relevant literature references. In compliance with the

Table 1. Thermophysical properties for blood and nanoparticles (Tripathi, Vasu, Bég, et al. 2021).

Properties	Blood	Gold (Au)	Silver (Ag)
$\rho(kg/m^3)$	1,063	19,320	10,500
k(W/mK)	4.92×10^{-1}	3.14×10^{2}	4.29×10^{2}
C_p (J/kgK)	3594	129	235
$\gamma(K^{-1})$	1.8×10^{4}	1.4×10^{5}	_
$\sigma(S/m)$	6.67×10^{-1}	4.1×10^{7}	_

U.S. Food and Drug Administration (FDA) guidelines, several studies including Hirsch et al. (2003), Connor et al. (2005), Guillemot et al. (2010), He et al. (2011), etc. have discussed the exceptional biocompatibility of gold and silver nanoparticles making them the preferred choices for stenosis treatment. Their biocompatibility ensures minimal adverse effects on biological systems, facilitating safer and more effective therapeutic outcomes. Also, Table 3 presents a structured comparison of different nanoparticles, detailing their biocompatibility and the specific reasons for their biocompatibility. This table systematically highlights the role of chemical stability, toxicity, and biodegradability in determining the suitability of nanoparticles for biomedical applications. Based on Tables 2 and 3, gold and silver nanoparticles are highly valued in biomedical applications due to their stability, biocompatibility, and therapeutic potential, with gold nanoparticles excelling in targeted therapy and photothermal applications, while silver nanoparticles offer strong antimicrobial properties. Furthermore, gold and silver nanoparticles accumulate preferentially in tumor tissues with leaky blood vessels. This enhances drug delivery to the target site and reduces off-target effects (Austin et al. 2014; Ghazal et al. 2024; Gupta et al. 2024; Thakur and Kumar 2024). Therefore, the utilization of gold and silver nanoparticles in this study not only capitalizes on their superior thermophysical properties but also underscores their unmatched biocompatibility, drug delivery to targeted sites, and reduced off-target effects positioning them as optimal candidates for stenosis therapy.

An inspection of the existing literature reveals that the impact of gold and silver nanoparticles on the Newtonian dissipative flow dynamics within stenotic arteries, characterized by porous walls and convective wall heating, taking into account the viscous dissipation effects has not yet been examined. This omission highlights a significant limitation in the research, as viscous dissipation plays a crucial role in fluid flow dynamics, particularly in microcirculatory systems like arteries. The absence of this factor creates a research gap that warrants attention, as understanding the impact of viscous dissipation on blood flow with

Table 2. Comparison of different nanoparticles for biocompatibility, and potential biomedical applications with past studies.

Die se were stile iliter	Potential biomedical	Studies highlighting the treatment of
вюсотранинцу	applications	stenosis utilizing particular nanoparticles
Excellent	Potential for targeted therapy,	(Raju et al. 2024; Waqas et al. 2022, 2023)
	Photothermal ablation	(Hussain et al. 2022; Tang et al. 2023)
Good	Potential antimicrobial effects,	(Hussain et al. 2022; Waqas et al. 2022; 2023)
	Wound healing properties	(Li et al. 2021, 2022)
Generally good	Potential for imaging-guided	(Kozlov et al. 2022; Wang et al. 2024)
	Drug delivery, diagnostics	(Schneider and Lassalle 2017)
Generally good	Potential for targeted drug delivery,	(Chan et al. 2011; Shiozaki et al. 2016)
	Biomolecule delivery	(Akhlaghi et al. 2019)
Variable	Potential for sustained drug release,	(Agyare and Kandimalla 2014; Shi et al. 2023)
	Tissue regeneration	(Chan et al. 2011)
Generally good	Potential for bone tissue regeneration,	(Lan et al. 2014; Xiao et al. 2024)
	Drug delivery	(Hashemzadeh et al. 2024)
Moderate to good	Potential for drug delivery,	(Akbar 2015; Shahzad et al. 2024)
	Tissue engineering and Biosensing	(Nadeem and Ijaz 2015)
Generally good	Potential for targeted therapy,	(Wu et al. 2021; Islam et al. 2024)
	Diagnostic applications	(Kharlamov et al. 2015)
Generally good	Potential for targeted drug delivery,	(Badfar et al. 2020; Majee and Shit 2020)
	Hyperthermia therapy	(Varmazyar et al. 2020; Bhatti et al. 2022)
Variable	Potential antimicrobial effects,	(Zhang et al. 2020),
	Wound healing properties	(Shabbir et al. 2022)
Variable	Potential for photodynamic therapy,	(Zaman et al. (2018, 2019; Bian et al. 2023)
	Targeted drug delivery	(Ahmed and Nadeem 2016)
	Good Generally good Variable Generally good Moderate to good Generally good Generally good Variable	Biocompatibility Excellent Potential for targeted therapy, Photothermal ablation Good Potential antimicrobial effects, Wound healing properties Generally good Potential for imaging-guided Drug delivery, diagnostics Generally good Potential for targeted drug delivery, Biomolecule delivery Variable Potential for sustained drug release, Tissue regeneration Generally good Potential for bone tissue regeneration, Drug delivery Moderate to good Potential for drug delivery, Tissue engineering and Biosensing Generally good Potential for targeted therapy, Diagnostic applications Generally good Potential for targeted drug delivery, Hyperthermia therapy Variable Potential antimicrobial effects, Wound healing properties Variable Potential for photodynamic therapy,

Table 3. Reason for particular biocompatibility of different nanoparticles.

Nanoparticle	Biocompatibility	Reason for biocompatibility
Gold nanoparticles	Excellent	Chemically inert, high stability and ease of surface functionalization (Kadhim et al. 2021; Kus- Liśkiewicz et al. 2021)
Silver nanoparticles	Good	Highly stable in biological fluids due to surface modifications but induces cytotoxicity at high concentrations (Ahamed et al. 2011; Arshad et al. 2024)
Iron oxide nanoparticles	Generally good	High stability in biological environments but potential oxidative stress and cytotoxicity at high concentrations (Ansari et al. 2024; Tadić et al. 2025)
Lipid nanoparticles	Generally good	Highly stable due to their biodegradable and amphiphilic nature, Low toxicity as they are composed of biocompatible lipids similar to natural cell membranes (Arabestani et al. 2024; Dhayalan et al. 2024)
Polymeric nanoparticles	Variable	Stability depends on the polymer type, Low toxicity for biodegradable polymers, but non- degradable ones may cause long-term accumulation and potential cytotoxicity (Encinas- Basurto et al. 2024; Geszke-Moritz and Moritz 2024)
Calcium phosphate nanoparticles	Generally good	Highly stable and bioresorbable, mimicking the natural mineral phase of bones and teeth, Low toxicity due to natural presence in the body (Khalifehzadeh and Arami 2020; Sokolova and Epple 2021)
Carbon nanotubes	Moderate to good	Highly stable with strong mechanical and electrical properties, but prone to aggregation if not functionalized, surface functionalization improves biocompatibility (Chłopek et al. 2006; Smart et al. 2006)
Silicon nanoparticles	Generally good	High chemical and thermal stability, porous silicon nanoparticles improve drug loading and controlled release, Generally low toxicity (Asefa and Tao 2012; Shahbazi et al. 2013)
Magnetic nanoparticles	Generally good	High stability in biological environments, often coated to enhance dispersibility and prevent aggregation, toxicity depends on coating (Markides et al. 2012; Reddy et al. 2012)
Zinc oxide nanoaprticles	Variable	Stable in biological environments but can degrade under certain pH conditions, releasing zinc ions, which may cause cytotoxicity at high concentrations (Barman 2015; Mahalakshmi et al. 2020)
Titanium dioxide nanoparticles	Variable	High chemical stability and resistance to degradation, but may accumulate in biological tissues over time, Prolonged exposure may induce oxidative stress and inflammation, especially in high doses (Ziental et al. 2020; Rashid et al. 2021)

nanoparticles is essential for a more accurate depiction of physiological conditions. Viscous dissipation (internal friction) arises since blood is highly viscous and heat-conducting, and this effect can also contribute to hyperglycemia (Çinar et al. 2001). The incorporation of viscous dissipation effects into the study would not only enhance its completeness but also contribute significantly to the existing literature by providing insights into how it influences velocity and heat transfer characteristics within stenotic arteries This is the focus of the present work which is motivated by ongoing research in the application of nanoparticles for the treatment of cardiovascular diseases. Metallic nanoparticles of gold and silver typically ranging from 1 to 100 nm in size have been utilized in the current study. The present study accounts for the deformability of arterial walls, including their stretching/shrinking, and wall curvature effects. Darcy's model is utilized to simulate bulk impedance in the porous medium (Khaled and Vafai 2003). The transport of substances like low-density lipoprotein (LDL) through stenotic walls under hypertension is considered, highlighting the significance of porous arteries in facilitating substance exchange between blood and tissues (Dabagh et al. 2009). Additionally, the study incorporates viscous dissipation and convective wall heating effects to account for blood viscosity and realistic wall thermal physics (Hussain et al. 2024). Conservation equations for mass, momentum, and heat, along with boundary conditions, are formulated using Tiwari-Das nanoscale model (Tiwari and Das 2007) and viscoelastic models. The resulting nonlinear boundary value problem is solved computationally. The study visualizes the effects of various physical parameters on transport characteristics using graphical representations, including three-dimensional contour plots, and provides a thorough discussion of the findings. The originality of this study includes the simultaneous consideration of gold/silver nanoparticles, wall curvature effect, convective wall heating, arterial wall permeability, Darcy porous drag effects, and viscous dissipation with Newtonian characteristics in stenotic hemodynamics. The simulations are expected to enhance the understanding of nano-hemodynamics in diseased arteries and pave the way for further research avenues, such as turbulent flow and fluid-structure interaction investigations.

2. Nano-blood model

2.1. Geometry of the stenosed artery

A uniform, 2-D flow of blood with gold and silver nanoparticles is examined through a stenotic artery under viscous dissipation. Since the cylindrical coordinates are naturally suited to describe the radial symmetry present in arterial geometry, particularly in cylindrical vessels like arteries, therefore axisymmetric cylindrical geometry is taken into account. This symmetry simplifies the mathematical description of the problem, reducing it from three dimensions to two, thus making the problem computationally more tractable. This geometry holds significant relevance in both medical and industrial contexts. Arterial stenosis refers to the narrowing of blood vessels, often due to the accumulation of plaque, which can lead to restricted blood flow. The understanding of the flow dynamics within stenosed arteries is crucial for various medical applications, such as diagnosing and treating cardiovascular diseases. Additionally, insights gained from studying arterial stenosis have implications for industries involved in medical device development, drug delivery systems, and biomedical engineering. Patankar (2018) explained the proper choice of coordinates for the problem under study according to the flow geometry in real life.

The geometry of arterial stenosis for the posed problem is documented in Figure 1. The stenosis is assumed to be symmetric, meaning that the arterial walls contract and expand in a predictable manner. The arterial length of stenosis is considered $\frac{L_0}{2}$. If the extreme height of stenosis is λ , the width of the unobstructed region is $2R_0$, then the radius R(x) of the stenosed artery is given by

$$R(x) = \begin{pmatrix} R_0 - \frac{\lambda}{2} \left(1 + \cos\left(\frac{4\pi x}{L_0}\right) \right), & -\frac{L_0}{4} < x < \frac{L_0}{4} \\ R_0, & \text{Otherwise} \end{pmatrix}.$$
(1)

It represents a realistic and biologically relevant arterial narrowing. The smooth nature of this function eliminates sudden jumps or discontinuities in arterial radius, which could lead to unrealistic flow behavior.

2.2. Mathematical modeling of the posed problem

Blood is contemplated as a Newtonian incompressible fluid that is flowing along the x-axis and the r-axis is taken orthogonal to the flow of blood.

The dictating governing equations of continuity, mass and momentum are given by Sarwar and Hussain (2021) and Waqas et al. (2022)

$$\frac{\partial(ru)}{\partial x} + \frac{\partial(rv)}{\partial r} = 0, \tag{2}$$

$$\left(u\frac{\partial}{\partial x} + v\frac{\partial}{\partial r}\right)u = \frac{\mu_{nf}}{\rho_{nf}}\frac{\partial}{r\partial r}(ru_r) - \frac{\sigma B(x)^2}{\rho_{nf}} - \frac{\mu_{nf}}{K}u, \tag{3}$$

$$\left(u\frac{\partial}{\partial x} + v\frac{\partial}{\partial r}\right)T = \frac{k_{nf}}{(\rho C_p)_{nf}}\frac{\partial}{r\partial r}(rT_r) - \frac{1}{(\rho C_p)_{nf}}(q_r)_r, \tag{4}$$

with boundary states

$$u = u_w, v = v_w, -k_f T_r = h_f (T_f - T_r) atr = R, u \to 0, \quad T \to T_\infty \text{ as } r \to \infty$$
 (5)

In arterial blood flow, heat transfer plays a crucial role in maintaining the thermal equilibrium of the system, which is vital for the proper functioning of the circulatory system. The boundary conditions

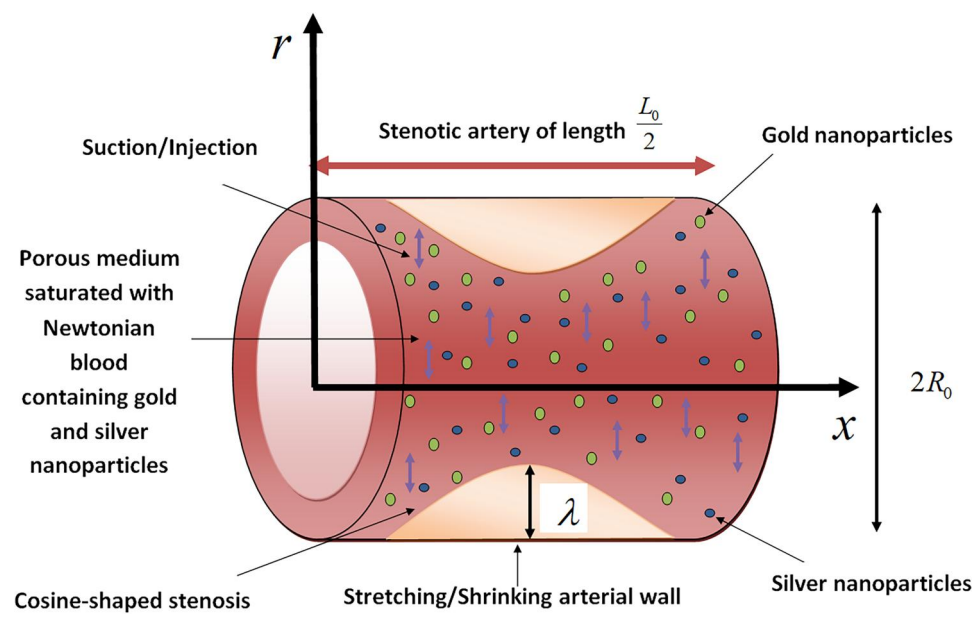


Figure 1. Geometry of arterial stenosis with saturated porous blood containing gold and silver nanoparticles.

specified in Equation (5) ensure that the velocity components u and v are respectively equal to u_w and v_w , the velocity components at the wall (r = R). Moreover, the equation $-k_f T_r = h_f (T_f - T_r)$ describes the heat transfer between the arterial blood and the surrounding tissues using Newton's Law of Cooling, which states that the rate of heat transfer between a fluid and a solid surface is directly proportional to the temperature difference between the fluid and the surface.

The term $h_f(T_f - T_r)$ represents the rate of heat transfer between the arterial blood and the surrounding tissues due to convection. The temperature difference $(T_f - T_r)$ drives the heat transfer from blood to tissues while h_f is the heat transfer coefficient. This coefficient represents the efficiency of heat transfer between the blood and the tissues. A higher heat transfer coefficient means heat can transfer more easily between the blood and the tissues. $-k_fT_r$ represents the rate of heat transfer between the arterial blood and the surrounding tissues due to conduction. This term indicates that heat is transferred through the tissues via conduction, with the rate of transfer being proportional to the temperature gradient T_r (higher temperature) within the tissues.

In the current study, a Newtonian blood-based model that mimics the flow characteristics of blood mixed with nanoparticles has been taken into consideration. The motivation for selecting this fluid model stems from its relevance to biomedical engineering and healthcare applications, where understanding the behavior of blood flow under various conditions, such as arterial stenosis, is critical. The incorporation of

nanoparticles (gold and silver) into the blood aims to explore the potential enhancements or alterations in flow behavior, heat transfer, and other relevant parameters. Some real-world applications of this fluid model include drug delivery systems, medical diagnostics, and understanding physiological phenomena such as microcirculation. Figure 2 illustrates a graphical abstract of the current study.

Rosseland's approximation for the radiative heat flux q_r is derived under the assumption that the medium absorbs and emits radiation efficiently and is given by

$$q_r = -\frac{4\sigma^*}{3k^*} (T^4)_r, (6)$$

Here, σ^* represents the Stefan-Boltzman constant and k^* represents the mean absorption coefficient. Also, by the Taylor series, the approximated value of (T^4) is given by

$$\left(T^4 \approx 4TT_{\infty}^3 - 3T_{\infty}^4\right),\tag{7}$$

2.3. Modeling of arterial wall as a saturated porous medium

Modeling the arterial walls as a porous medium enhances physiological realism by accounting for the natural micro-porous structure of tissues, which includes capillaries, interstitial spaces, and a semipermeable endothelium. This approach improves the simulation of mass and heat transfer processes-vital for capturing the exchange of drugs or thermal energy between blood and tissue—and enables

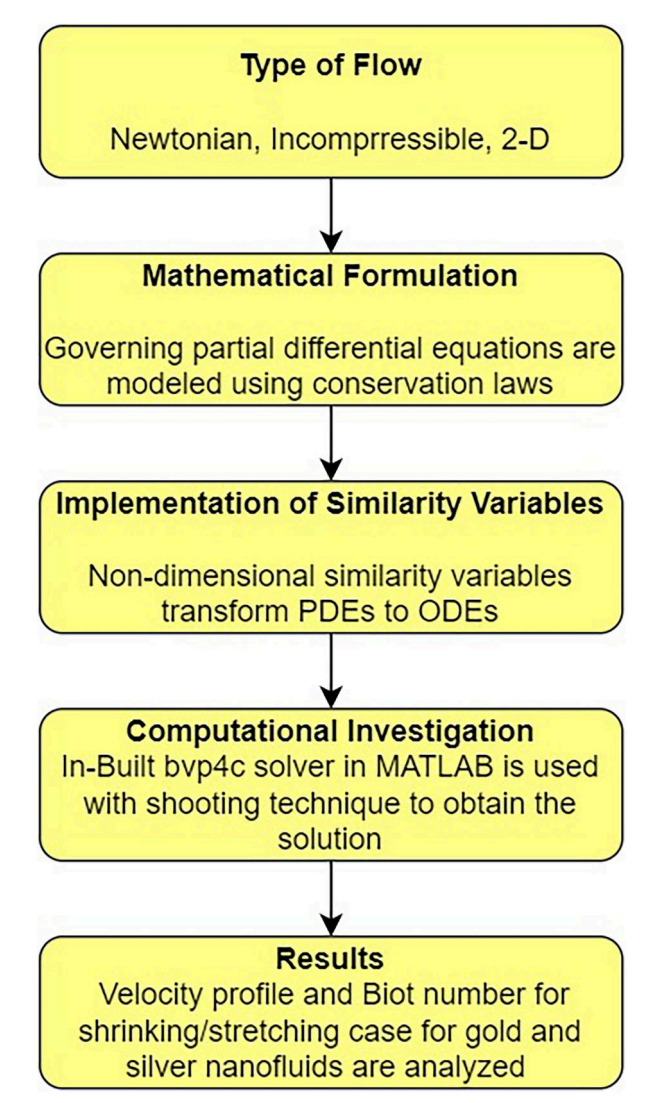


Figure 2. Flowchart of the problem.

incorporation of permeability effects that can vary between healthy and diseased states. Additionally, representing the arterial wall as a porous medium facilitates a more accurate depiction of complex fluid-structure interactions, thereby allowing the model to predict localized shear stresses and temperature gradients that influence cellular responses and overall vascular health.

Darcy's law (Beliaev and Kozlov 1996) provides a simple yet robust framework for modeling flow resistance within porous media by establishing a linear relationship between flow velocity and pressure gradient, which simplifies the integration of additional drag forces into the momentum equations. To simulate the physiological conditions in which the arterial wall is not a perfect solid but has a porous structure due to microchannels in the endothelium or the transport of substances like lipids, Darcy's drag model

is adopted (Beliaev and Kozlov 1996). In the porous region, the flow resistance is modeled by an additional Darcy drag term $\frac{\mu_{nf}K}{u}$ in the momentum Equation (3). The permeability coefficient K quantifies the ease with which the nano-blood permeates the porous arterial wall.

2.4. Doping of gold and silver nanoparticles in human blood

The study is carried out by doping human blood with gold and silver nanoparticles. Gold and silver nanoparticles are selected based on their superior biocompatibility and thermal conductivity, which are critical for biomedical applications such as targeted drug delivery and hyperthermia treatment as clear from Tables 2 and 3 and discussed in detail in the Introduction section. Gold nanoparticles, in particular, exhibit higher thermal conductivity, making them more effective in enhancing heat transfer while antimicrobial properties of silver nanoparticles make them suitable for doping in human blood.

The thermophysical properties of nanofluids as described by Tiwari and Das (2007) nanofluid model are given by

$$\mu_{nf} = \mu_{f} (1 - \phi)^{-2.5}, \rho_{nf} = \rho_{f} (1 - \phi) + \phi \rho_{s},
(\rho c_{p})_{nf} = (\rho c_{p})_{f} (1 - \phi) + \phi (\rho c_{p})_{s},
k_{nf} = k_{f} \left[\frac{k_{s} + 2k_{f} - 2\phi (k_{f} - k_{s})}{k_{s} + 2k_{f} + 2\phi (k_{f} - k_{s})} \right]$$
(8)

Based on these properties, the following parameters are defined:

$$A_{1} = (1 - \phi) + \phi \frac{\rho_{s}}{\rho_{f}}, A_{2} = (1 - \phi) + \phi \frac{(\rho C_{p})_{s}}{(\rho C_{p})_{f}},$$

$$A_{3} = \frac{k_{s} + 2k_{b}f - 2\phi(k_{b}f - k_{s})}{k_{s} + 2k_{b}f + 2\phi(k_{b}f - k_{s})}$$
(9)

Equation of continuity (1) is satisfied by introducing stream function ψ as follows:

$$u = \frac{1}{r} \frac{\partial \psi}{\partial r}, v = -\frac{1}{r} \frac{\partial \psi}{\partial x}.$$
 (10)

2.5. Introduction of non-dimensional variables

The dimensional analysis of Equations (3) and (4) and utilization of Buckingham's pi theorem (Hanche-Olsen 2004) leads to the following non-dimensional functions (Sarwar and Hussain 2021) (see Langhaar (1951)):

$$u = \frac{u_0 x}{L_0} f'(\eta), v = \frac{R}{r} \sqrt{\frac{u_0 v_f}{L_0}} f(\eta),$$

$$\theta(\eta) = \frac{T - T_\infty}{T_w - T_\infty}, \eta = \frac{r^2 - R^2}{2R} \sqrt{\frac{u_0}{v_f L_0}},$$
(11)

Utilizing the functions in Equation (11), Equations (3) and (4) transform to:

$$\frac{\left[(1+2\gamma\eta)f'''+2\gamma f''\right]}{(1-\phi)^{2.5}A_1} + ff'' - f^{2'} - Mf' - \beta f' = 0, \quad (12)$$

$$\frac{A_3}{\text{PrA}_2} \left[(1 + 2\gamma \eta)\theta'' + 2\gamma R d\theta' \right] + f\theta' - f'\theta = 0, \quad (13)$$

with boundary states

$$f(0) = f_w, f'(0) = \lambda, \theta'(0) = -Bi(1 - \theta(0)),$$

$$f'(\eta) \to 0, \theta(\eta) \to 0 \text{ as } \eta \to \infty$$
 (14)

Here f_w corresponds to mass flux (suction/injection) and λ accounts for the deformability of arterial wall with $\lambda = 1$ and $\lambda = -1$ representing stretching and shrinking respectively.

The non-dimensional functions which arise as a consequence of defining non-dimensional functions in Equation (11) are presented as follows:

$$\Pr = \frac{k_f}{(\mu C_p)_f}, \gamma = \sqrt{\frac{\nu_f L_0}{u_0 R^2}}, Rd = \frac{4\sigma^* T_{oo}^3}{k^* k}, M = \frac{\sigma B_0^2}{c\rho_{nf}}$$

$$\beta = \frac{\mu_f L_0}{\rho_f u_0 K}, Bi = \sqrt{\frac{\nu_f}{b}} \frac{h_f}{k_{nf}}, C_f = \frac{\tau_w}{\frac{1}{2}\rho_f U_w^2}, Nu = \frac{xq_w}{k_f (T_w - T_\infty)}$$
(15)

where Pr is the Prandtl number, γ represents the flow parameter, Rd is the thermal radiation parameter, M is the magnetic parameter, Bi is the Biot number, C_f represents the skin friction and Nu_x represents the Nusselt number.

In light of the dimensionless variables

$$f^* = \frac{R(x)}{R_0}$$
 and $\epsilon = \frac{\lambda}{R_0}$ (16)

the non-dimensional form of cosine-shaped stenosis given in Equation (1) emerges as

$$f^* = \begin{pmatrix} 1 - \frac{\epsilon}{2} (1 + \cos(4\pi\tilde{x})), -\frac{1}{4} < \tilde{x} < \frac{1}{4} \end{pmatrix} .$$

$$1, \text{ Otherwise}$$

$$(17)$$

where $x = \frac{\tilde{x}}{I_0}$.

2.6. Engineered parameters

Nusselt number, skin friction, heat flux, and shear stress are given by

$$Nu = \frac{-xq_w}{k_f(T_{\infty} - T_w)}, C_f = \frac{2\tau_w}{\rho_f U_w^2},$$
 (18)

$$q_{w} = -k_{nf} \frac{\partial T}{\partial r} \bigg|_{r=R}, \tau_{w} = \mu_{nf} \frac{\partial u}{\partial r} \bigg|_{r=R}.$$
 (19)

The governing parameters, coefficients corresponding to skin friction, and Nusselt number are described as

$$Re_x^{1/2}C_f = \frac{1}{(1-\varphi)^{2.5}}f'(0),$$
 (20)

$$Re_x^{-1/2}Nu_x = -\frac{k_{nf}}{k_f}Rd\theta'(0).$$
 (21)

3. Method of solution

The bvp4c technique, part of MATLAB's Boundary Value Problem (BVP) solver suite, is an efficient solver that employs a finite difference method to solve systems of ordinary differential equations (ODEs) subject to boundary conditions. The complex nature of the present problem enables the utilization of this technique. In this technique, the spatial domain is discretized into a grid, and the derivatives in the ODEs using finite differences. The resulting system of algebraic equations is then solved iteratively to obtain a numerical solution that satisfies both the ODEs and the boundary conditions. The solver adjusts the solution iteratively until it converges to a satisfactory result, typically using Newton's method or similar iterative techniques. This process involves updating the solution at each grid point based on the residuals of the ODEs and boundary conditions, aiming to minimize these residuals to zero. The solver continues iterating until the solution converges within a specified tolerance level. Overall, the bvp4c technique provides a robust and efficient approach to solving boundary value problems arising in various scientific and engineering applications.

The coupled non-linear differential equations obtained are first converted to the following firstorder system of differential equations as follows:

$$\begin{cases}
f = z_1, f' = z_2, f'' = z_3, f''' = z'_3, \\
\theta = z_4, \theta' = z_5, \theta'' = z'_5
\end{cases},$$
(22)

$$z_{3}' = \frac{-\frac{1}{(1-\phi)^{2.5}}[2\gamma z_{1}] - z_{1}z_{3} + z_{2}^{2} + Mz_{2} + \beta z_{2}}{\frac{1}{(1-\phi)^{2.5}A_{1}}(1+2\gamma\eta)},$$
 (23)

$$z_{5}' = \frac{-\frac{A_{3}}{\Pr A_{2}}[2\gamma R dz_{5}] - z_{1}z_{4} + z_{2}z_{4}}{\frac{A_{3}}{\Pr A_{2}}(1 + 2\gamma \eta)},$$
 (24)

with boundary states

$$z_{1}(0) = f_{w}, z_{2}(0) = \lambda, z_{5}(0) = -Bi(1 - z_{4}(0)), z_{2}(\eta) \to 0, z_{4}(\eta) \to 0 \text{ as } \eta \to \infty$$
 (25)

The bvp4c solver of MATLAB is then employed to find the solution of the above system of differential equations. Tolerance of order 10⁻⁶ is taken for precise results. bvp4c technique, like any numerical method,



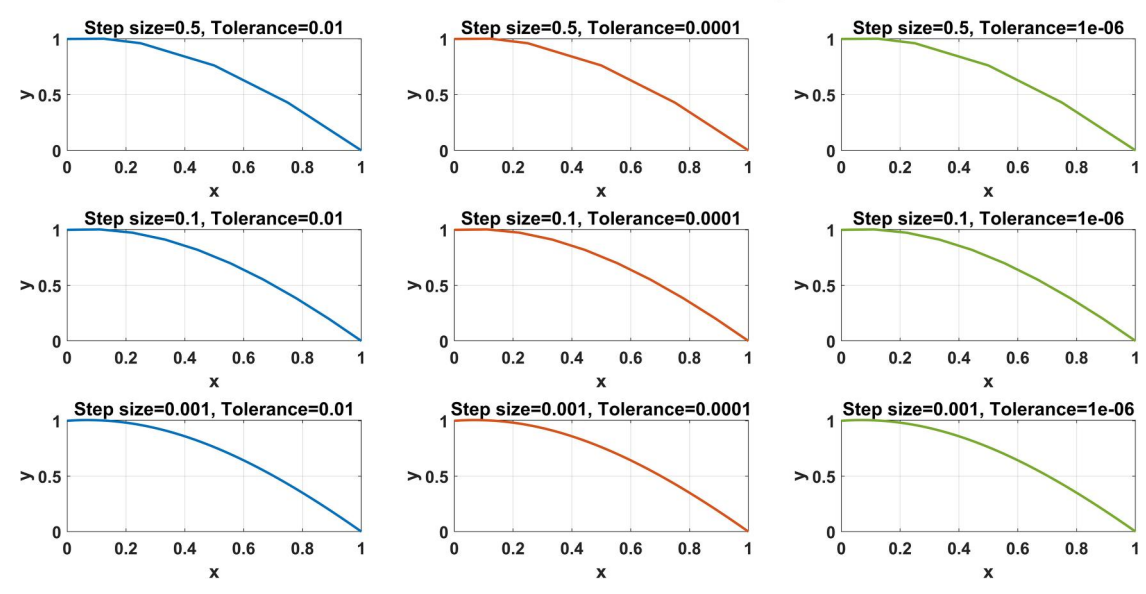


Figure 3. Effect of step size and tolerance on the convergence of solution.

has both advantages and limitations. It can handle a wide range of boundary value problems arising in different fields, including physics, engineering, and biology. The solver is generally robust and can handle stiff ODE systems, where traditional explicit methods may fail. Despite its robustness, the solver's convergence can be sensitive to the initial guess provided, particularly for complex problems. While versatile, bvp4c may not be suitable for certain specialized boundary value problems that require tailored numerical methods or algorithms. Depending on the problem's characteristics and discretization scheme, bvp4c may introduce numerical errors or inaccuracies, especially near discontinuities or singularities in the solution.

Also, in solving boundary value problems (BVPs) using the bvp4c function in MATLAB, both the step size and tolerance are critical factors that influence the convergence of the numerical solution. The step size determines the discretization of the independent variable (e.g. space or time) and affects the granularity of the numerical approximation. A smaller step size generally leads to a more accurate solution but may increase computational costs. On the other hand, the tolerance specifies the acceptable error or deviation from the exact solution. A lower tolerance requires the numerical solution to converge to a more precise solution before terminating the iterative process, resulting in higher accuracy but potentially requiring more computational effort. Conversely, a higher tolerance allows for a larger deviation from the exact solution and may lead to faster convergence but potentially less accurate results. Therefore, selecting appropriate values for both the step size and tolerance is crucial to achieving convergence efficiently while balancing accuracy and computational resources.

Figure 3 explores the effect of different step sizes and tolerances on the convergence of a numerical solution obtained by solving a boundary value problem (BVP) using the bvp4c function. The figure documented three different step sizes: 0.1, 0.05, and 0.01, and three different tolerance levels: 10^{-2} . 10⁻⁴, and 10⁻⁶. These values represent a range of discretization levels and acceptable error thresholds, respectively, allowing for a comprehensive exploration of the convergence behavior. The nested loops iterate over each combination of step size and tolerance, resulting in a total of nine subplots. Each subplot represents a specific combination of step size and tolerance. From these subplots, it is evident that decreasing the step size generally leads to a smoother and more accurate solution, as finer discretization captures more details of the underlying problem. Conversely, larger step sizes resulted in a more jagged or oscillatory solution, especially if the problem contains rapid changes or features that are not well-resolved by coarse discretization. Furthermore, lower tolerance levels require the numerical solution to converge to a more precise solution before terminating the iterative process. This often results in smoother and more accurate solutions while higher tolerance levels allow for a larger deviation from the exact solution, potentially leading to faster convergence but with reduced accuracy. Fine-tuning between the step size and

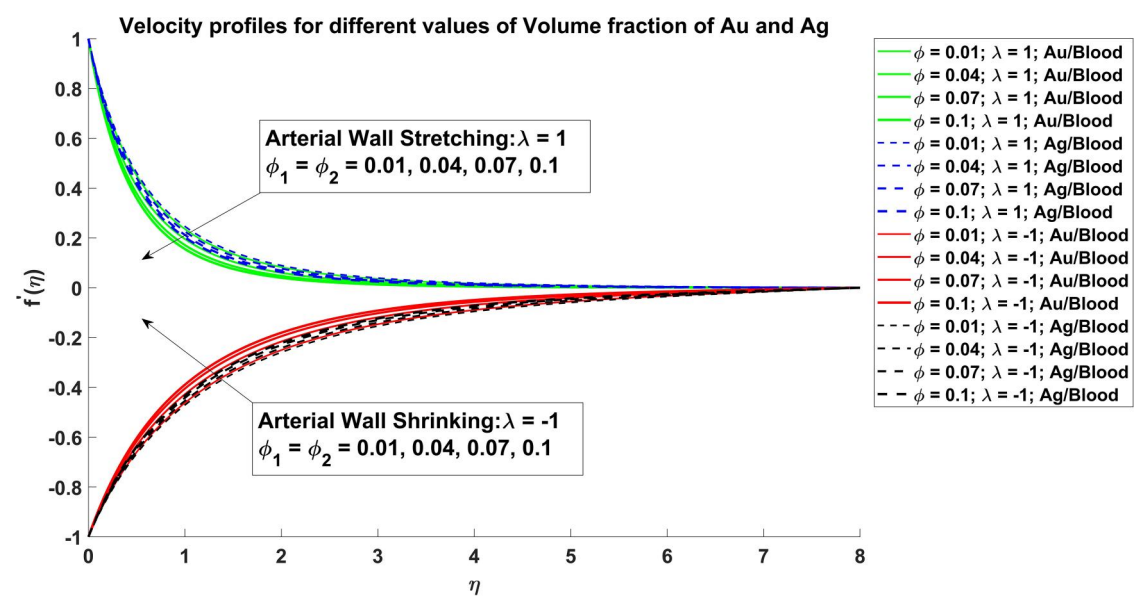


Figure 4. Velocity profiles for different values of volume fraction of Au and Ag.

tolerance level is crucial for achieving reliable and accurate results while balancing computational efficiency.

The velocity and temperature profiles for the posed problem are computed in the domain of [0, 6] by discretizing the domain with linspace(0, 6, 100) with tolerance of 10^{-6} .

4. Computational results and discussion

In this section, a detailed examination of the obtained results is conducted through a comprehensive analysis of graphs 4-19. These graphs depict the influence of various parameters on velocity profiles and thermal enhancement. Specifically, graphs 4-8 illustrate the impact of the volume fraction of nanoparticles of Au and Ag, suction/injection parameter, curvature flow parameter, magnetic parameter, and porosity parameter on velocity profiles. Graphs 9-13, on the other hand, portray the effects of the volume fraction of nanoparticles, suction/injection parameter, flow parameter, magnetic parameter, thermal radiation parameter, and Biot number on heat transfer enhancement. Furthermore, graphs 14-15 elucidate the influence of volume fraction on skin friction and Nusselt number. Both the Cases of stretching $\lambda = 1$ and shrinking $\lambda =$ -1 of the arterial wall are taken into account for Au/blood and Ag/blood nanofluids. Lastly, surface contour plots for stretching and shrinking cases for Nusselt number and skin friction are presented in graphs 16-19. Graphical analysis for equal amounts of volume fraction of nanoparticles ($\phi_1 = \phi_2$) of Ag and Au in the range $0.01 \le \phi_1 = \phi_2 \le 0.1$ is carried out.

Other flow parameters are taken in the range, suction/injection parameter $-0.3 \le f_w \le 0.3$, flow parameter $0.1 \le \gamma \le 0.3$, magnetic parameter $0.1 \le M \le 2.2$, radiation parameter $0.1 \le Rd \le 1.2$, and Biot number $1 \le Bi \le 2.2$. The numerical values associated with these pertinent parameters align with realistic benchmarks, thereby contributing to a nuanced understanding and analysis of fluid dynamics.

4.1. Velocity profiles

Figures 4–8 delineate the effects of diverse physical parameters on velocity profiles observed within gold-blood and silver-blood nanofluids, considering both the scenarios of stretching ($\lambda=1$) and shrinking ($\lambda=-1$) arterial walls.

Figure 4 illustrates the evolution of dual velocity solutions concerning the influence of the volume fraction of gold and silver nanoparticles in both stretching and shrinking arterial wall scenarios. As the volume fraction of gold and silver nanoparticles increases, the velocity of the nanofluid diminishes. This phenomenon primarily stems from the aggregation of silver and gold nanoparticles, altering the viscosity of the nano-blood and instigating a deceleration effect. In the stretching case ($\lambda = 1$), positive velocity values persist consistently, whereas in the shrinking case ($\lambda = -1$), negative values indicative of flow reversal are observed. Notably, the velocity values for silver-blood nanofluids surpass those of gold-blood nanofluids, attributed to variations in nanoparticle densities that impact viscosity differently. In the stretching case, monotonic decays in velocity

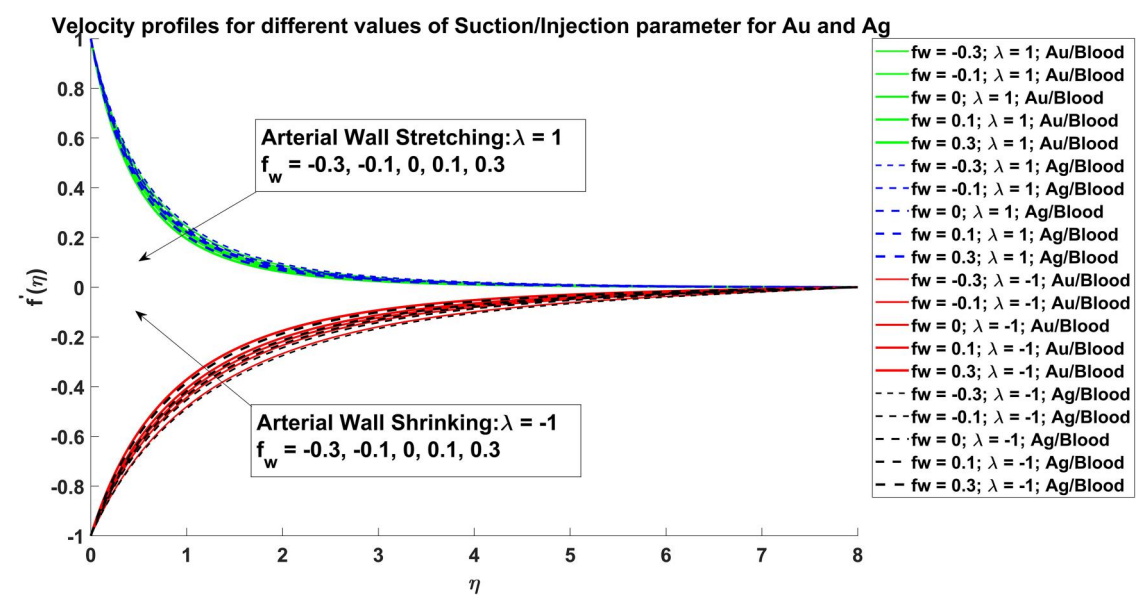


Figure 5. Velocity profiles for different values of suction/injection parameters for Au and Aq.

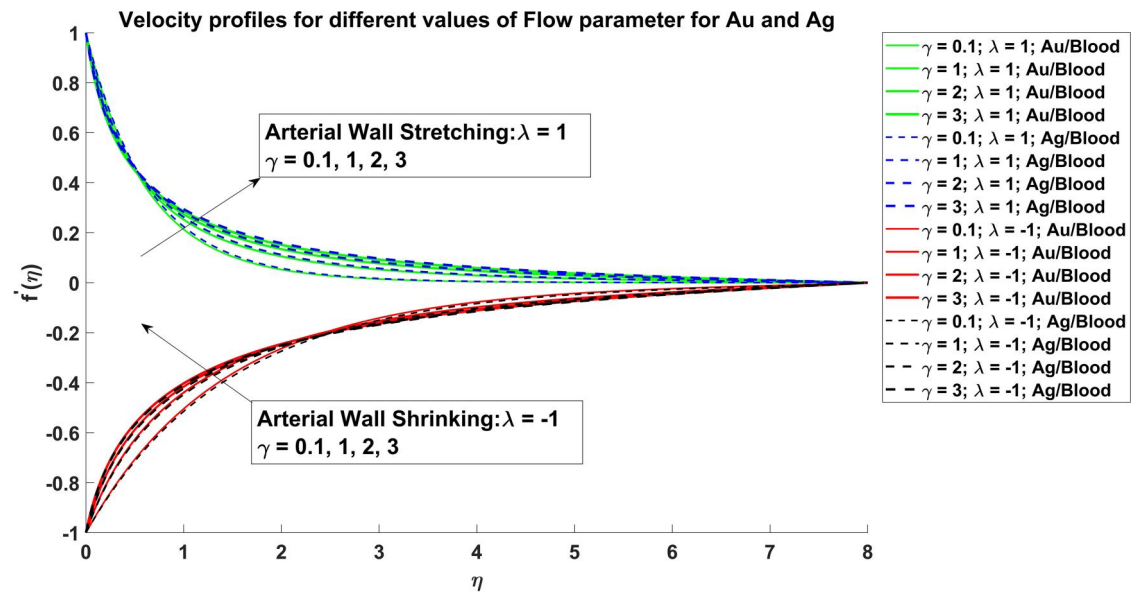


Figure 6. Velocity profiles for different values of flow parameters for Au and Ag.

are computed, while monotonic growth is evident in the shrinking case. The nature of wall deformation, represented by λ and solely affecting the wall velocity boundary condition in Equation (14), exerts a substantial influence on velocity distributions, as does the selection silver or gold nanoparticles. Consequently, hydrodynamic control can be achieved through the appropriate combination of nanoparticles and arterial wall stretching/shrinking. Overall, higher velocity magnitudes are computed with larger volume fractions of nanoparticles, which promote momentum diffusion within the regime. Figure 5 provides a visual representation of the influence of the lateral mass flux parameter, i.e. suction/injection parameter (f_w) , on the velocity distribution of nano-blood. This parameter is exclusively embedded within the wall velocity boundary condition, as outlined in Equation (14). Both gold-blood and silver-blood nanofluids showcase a decrease in velocity as the suction parameter $(f_w < 0)$ intensifies, while they exhibit a slight augmentation with a greater injection parameter $(f_w > 0)$. Hence, alterations in the wall mass flux distinctly impact velocity distribution, irrespective of whether the arterial wall is undergoing stretching or shrinking. Once again, significantly higher velocity magnitudes are linked to gold blood compared to silver blood. Figure 6 delves into the impact of flow parameters on the velocity profiles of gold-blood and silver-blood

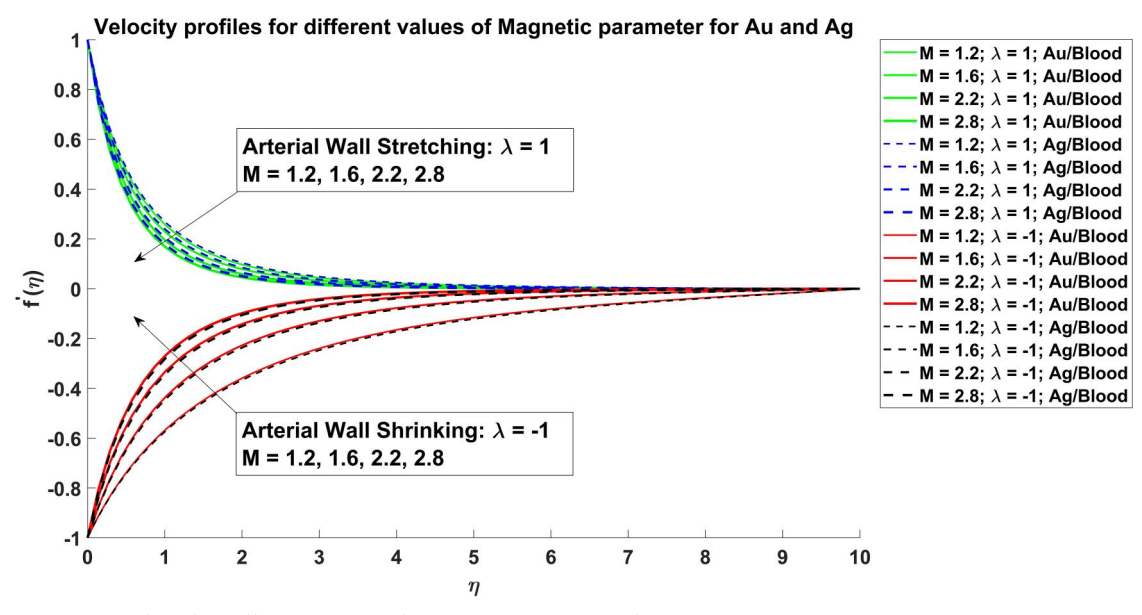


Figure 7. Velocity profiles for different values of magnetic parameters for Au and Ag.

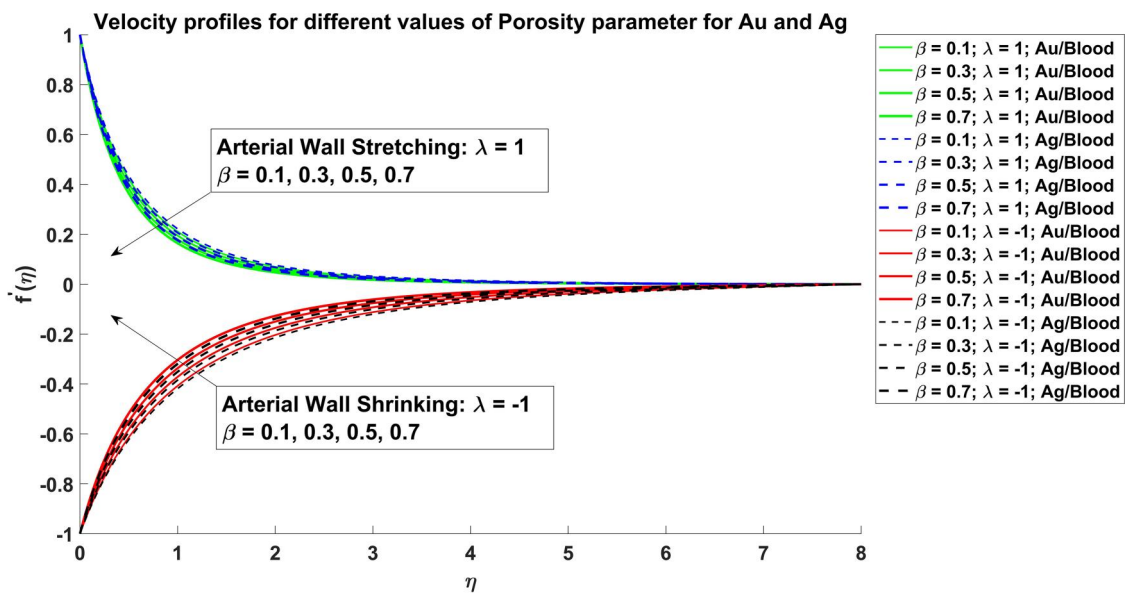


Figure 8. Velocity profiles for different values of porosity parameters for Au and Ag.

nanofluids, examining both shrinking and stretching scenarios. Notably, the velocity of nanofluids diminishes as the arterial curvature parameter, denoted by γ , increases, regardless of whether gold-blood or silver-blood nanofluids are considered. The elevations in the curvature parameter signify an augmentation in the radius of curvature, leading to a modification of the contact area between the nanofluid and the arterial wall. Consequently, the wall surface offers altered resistance to the motion of the nano-blood, inducing deceleration in the flow. The incorporation of wall curvature thus exerts a non-trivial influence on hemodynamic behavior, impacting both momentum and

energy equations where the curvature parameter appears in multiple terms. Also, a notable distinction is observed between the stretching and shrinking cases. Strong acceleration is evident in the stretching case compared to the shrinking case, and gold-blood tends to attain higher velocity magnitudes at any given value of the curvature parameter for stretching scenarios. The impact of magnetic parameter M on the velocity of gold-blood and silver-blood nanofluids is outlined in Figure 7. With an increase in the magnetic parameter, the magnetic forces exerted on the nanoparticles become stronger. These forces tend to induce clustering or aggregation of nanoparticles

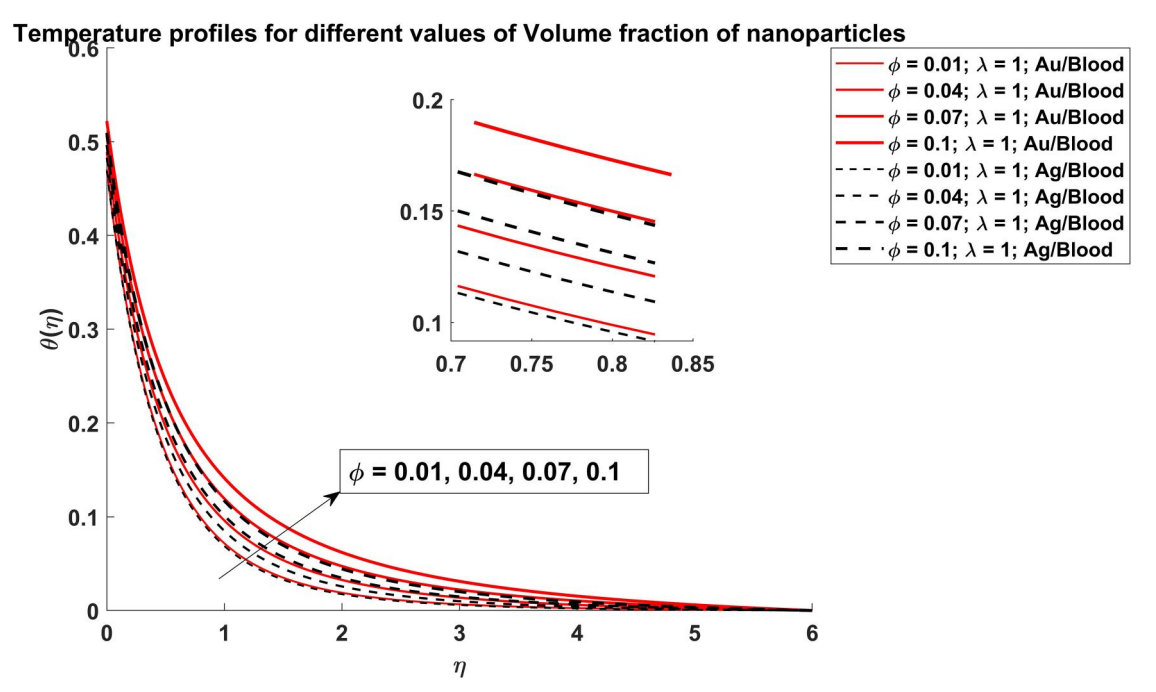


Figure 9. Temperature profiles for different values of volume fraction of Au and Ag.

along the direction of the magnetic field lines. As a result, the effective cross-sectional area available for fluid flow decreases due to obstruction by the clustered nanoparticles. This reduction in flow area leads to a decrease in fluid velocity. Also the presence of porous walls, the magnetic parameter affects the permeability of the porous medium. As the magnetic parameter increases, the magnetic forces acting on the nanoparticles within the porous medium intensify, leading to an increase in the Darcian resistance which results in a decrease in fluid velocity.

Figure 8 visualizes the impact of the porosity parameter, denoted by β , on the velocity profiles of goldblood and silver-blood nanofluids. The plots reveal a consistent trend i.e. as the permeability parameter increases, the velocity of both gold-blood and silverblood nanofluids decreases. The permeability parameter β is a key component in the linear Darcy term, represented as $-\beta f'$. As the value of β increases, the Darcian resistance experienced by the nanofluids within the porous medium intensifies, resulting in a corresponding reduction in permeability. This heightened resistance impedes the percolation of nanoblood through the porous medium, ultimately leading to deceleration in flow. Notably, silver-blood nanofluids tend to achieve higher velocities, both in stretching and shrinking scenarios, compared to goldblood. This observation underscores the differential behavior of the two types of nanofluids within the porous medium environment.

4.2. Temperature profiles

Figures 9-13 depict the temperature distributions within the stenosed artery, showcasing variations in nanoparticle volume fraction ϕ , Biot number Bi, curvature flow parameter γ , thermal radiation parameter Rd, and magnetic parameter M. These variations are observed specifically in the scenario of a stretching arterial wall ($\lambda = 1$), considering both gold-blood and silver-blood nanofluids. Figure 9 reveals a significant elevation in temperature magnitudes with increasing nanoparticle volume fraction of gold and silver nanoparticles. This temperature surge in goldblood and silver-blood nanofluids can be attributed to the exceptional thermal conductivity exhibited by gold and silver nanoparticles, as detailed in Table 1. Notably, substantially higher temperatures attained in the case of Au-blood as compared to Agblood. Also, a phenomenon of temperature overshoot near the arterial wall is observed, which diminishes with escalating volume fraction. These plots affirm the efficacy of nanoparticle utilization for thermal enhancement purposes. Figure 10 embellishes the impact of the mass flux (suction/injection) parameter on the temperature of Ag/blood and Au/blood nanofluids. The suction/injection parameter f_w serves as a crucial factor in governing the convective heat transfer process occurring within the stenosed artery. An increase in the suction parameter tends to enhance the flow velocity which intensifies the convective heat

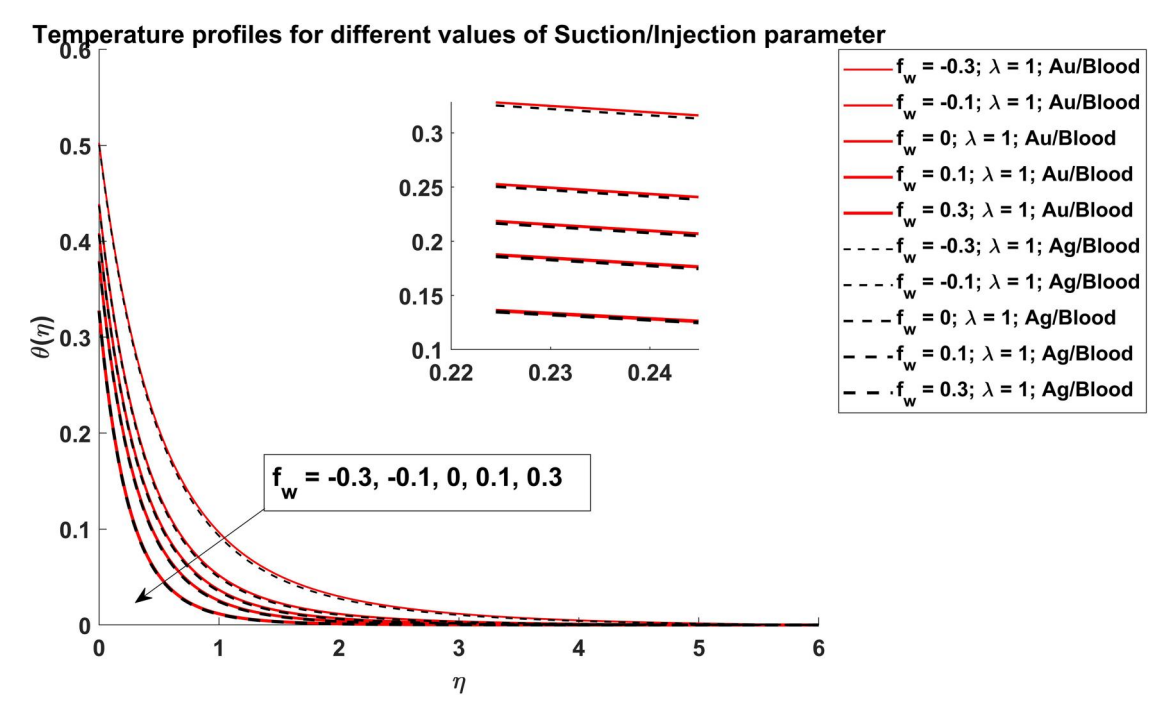


Figure 10. Temperature profiles for different values of suction/injection parameters for Au and Aq.

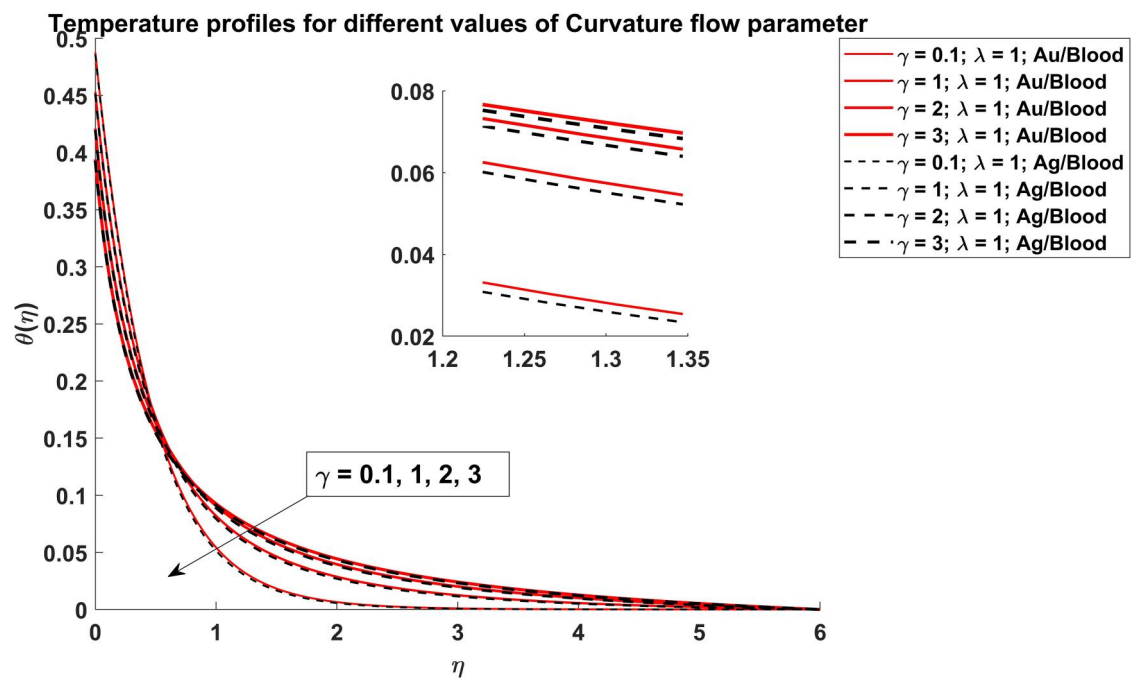


Figure 11. Temperature profiles for different values of flow parameters for Au and Aq.

transfer rate. This elevated fluid motion promotes efficient heat dissipation, leading to a more uniform temperature distribution along the arterial wall. Conversely, variations in the injection parameter exert contrasting effects on the temperature profiles. The augmentation in the values of the injection parameter results in a reduction of flow velocity, thereby diminishing the convective heat transfer rates. This

diminished flow velocity impedes the dispersion of heat within the arterial system, leading to localized temperature elevations, particularly in regions proximal to the stenosis.

Figure 11 explores the influence of the flow curvature parameter on the temperature profiles of goldblood and silver-blood nanofluids within the porous stenosed artery considering the effect of viscous

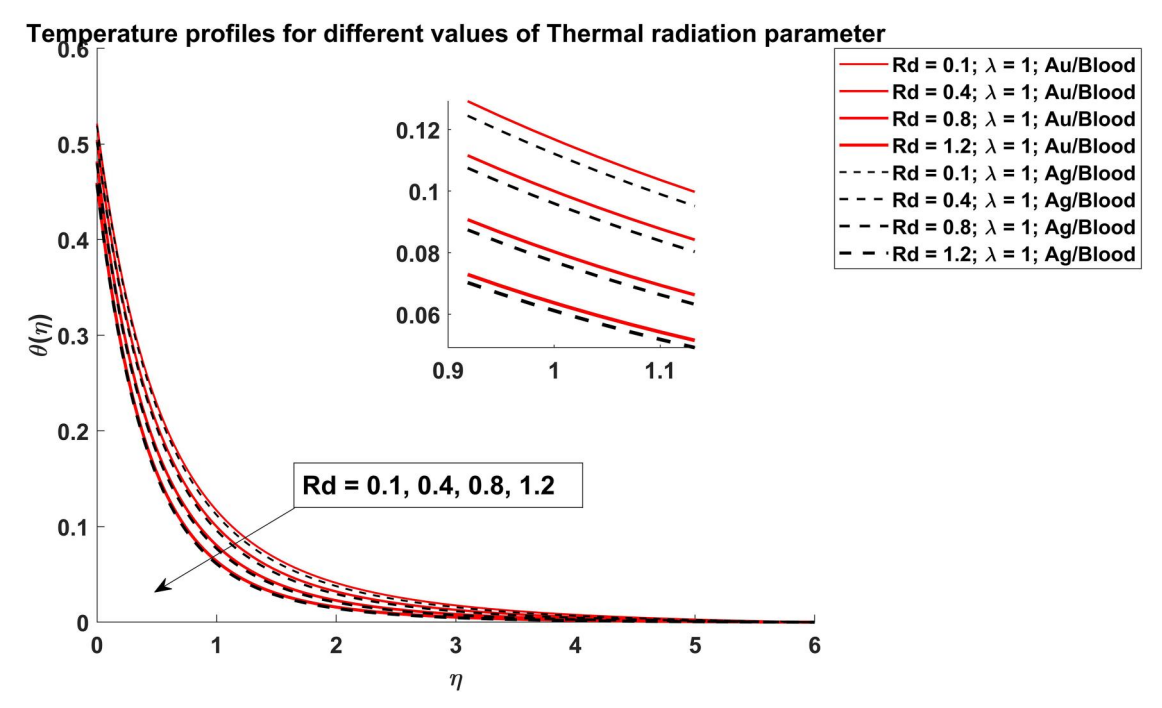


Figure 12. Temperature profiles for different values of radiation parameters for Au and Ag.

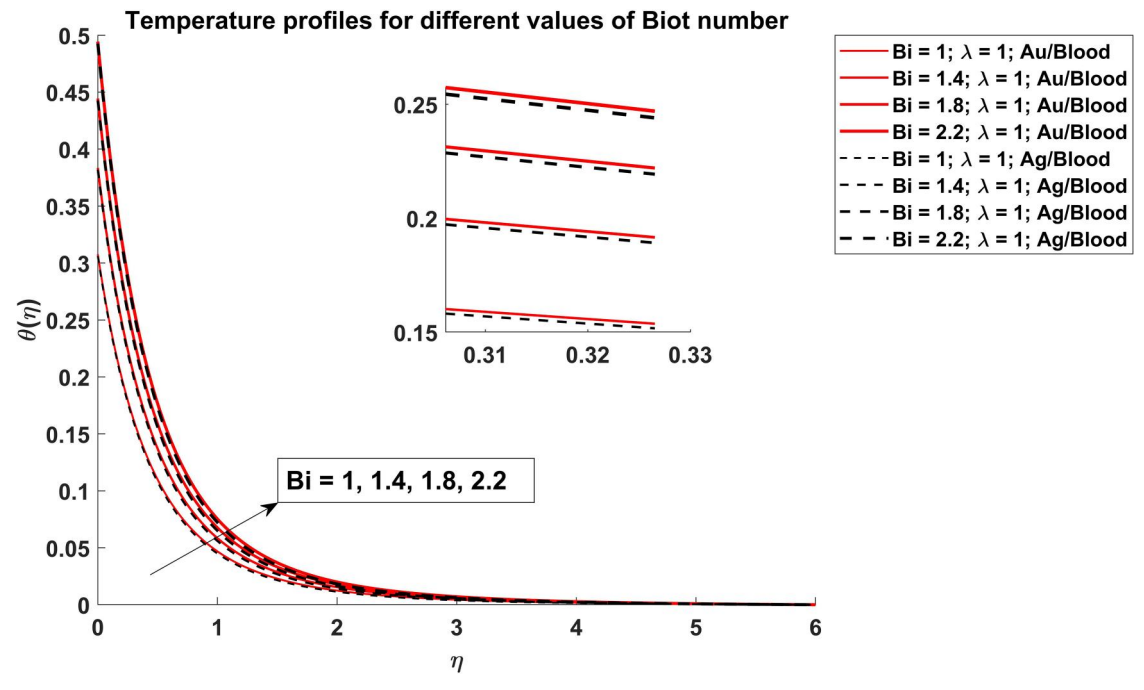


Figure 13. Temperature profiles for different values of Biot number for Au and Ag.

dissipation. Elevated temperatures are observed with larger curvature values for both the gold-blood and silver-blood nanofluids. The arterial curvature parameter, denoted by γ , prominently features in various terms within the energy equation (Eqn. 14), incorporating considerations for porous medium effects and viscous dissipation. These terms encompass expressions $\frac{A_3}{\Pr A_2}(1+2\gamma\eta)\theta''$ and $\frac{A_3}{\Pr A_2}(2\gamma Rd\theta')$. The magnification of curvature dynamically alters the contact

surface area between the percolating nano-blood and the arterial wall within the porous medium framework. This modification significantly impacts heat transfer dynamics between the bulk flow and the boundary, thereby instigating a notable reduction in temperatures and engendering a pronounced heating effect. Furthermore, similar temperature magnitudes are computed for both gold-blood and silver-blood nanofluids, highlighting the consistent influence of

arterial curvature on thermal behaviors within the stenosed artery, while accommodating the intricate interactions of the porous medium and the dissipative effects induced by viscous forces. Figure 12 establishes the relation between thermal radiation parameter and temperature of Au/blood and Ag/blood nanofluids. The rise in the value of the thermal radiation parameter causes the temperature profiles to go down as temperature distribution expands. Since with the increase in thermal radiation parameter, the contribution of radiative heat transfer becomes more pronounced. This radiation tends to facilitate heat dissipation from the nanofluids to their surroundings. Consequently, a higher thermal radiation parameter leads to more efficient heat removal, resulting in a decrease in temperature. Also, porous walls of the artery act as insulators, hindering heat transfer between the nanofluids and the surrounding environment. Additionally, viscous dissipation within the flowing nanofluids converts mechanical energy into heat, leading to an overall decrease in the temperature. The impact of the Biot number on temperature profiles is depicted in Figure 13. With regard to both gold-blood and silver-blood nanofluids, an increase in the thermal Biot number yields a pronounced adverse effect on temperatures, leading to a significant reduction. The Biot number denoted by Bi, is defined as the ratio between the resistance to heat conduction within the arterial wall and the resistance to heat convection at the wall's surface. It solely influences the thermal wall boundary condition, as seen in Equation (15), expressed as $\theta'(0) = -Bi(1 - \theta(0))$. When the Biot number exceeds 1, the rate of thermal conduction within the solid arterial wall interior becomes slower compared to thermal convection, thus impeding heat diffusion in the nano-blood and inducing a cooling effect. This effect is accentuated by the presence of porous walls within the artery, which further hinders heat transfer between the nanofluids and the surrounding environment. Additionally, the contribution of viscous dissipation within the nanofluids amplifies this cooling effect by converting mechanical energy into heat, contributing to the overall reduction in temperatures. Furthermore, it's noteworthy that the temperature of the gold-blood nanofluid consistently surpasses that of the silver-blood nanofluid for any given value of nanoparticle volume fraction, ϕ . This temperature difference can be attributed to variations in the thermal properties of gold and silver nanoparticles, as well as their interactions with the arterial wall and surrounding environment, further elucidating the intricate interplay between nanoparticle

characteristics, arterial wall properties, and heat transfer phenomena within the stenosed artery.

The alterations in temperature profiles of gold-blood and silver-blood nanofluids may hold significant implications for tumor treatment via hyperthermia, a method that necessitates elevated temperatures to effectively eradicate tumor cells. One promising approach involves the utilization of drugs loaded with nanoparticles, which can be precisely delivered to targeted sites within the body. On reaching these sites, manipulation of the blood temperature can be achieved using parameters such as volume fraction of nanoparticles, mass flux parameter, thermal radiation parameter, and Biot number. This manipulation leads to the generation of thermal energy within the bloodstream, which subsequently aids in the targeted destruction of tumors. Moreover, hyperthermia has emerged as a potential strategy for preventing the recurrence of stenosis, a narrowing of blood vessels often associated with various cardiovascular conditions. The therapeutic application of hyperthermia in such cases requires further exploration, particularly through advanced computational fluid dynamics (CFD) simulations. These simulations play a crucial role in elucidating the complex fluid dynamics and heat transfer processes occurring within biological systems, thus paving the way for the development of more effective clinical treatments.

4.3. Arterial wall skin friction and Nusselt number

Figures 14 and 15 illustrate the impacts of heat transfer i.e. Nusselt number and coefficient of arterial wall skin friction for stenosed artery. Specifically, Figure 14 depicts the behavior of the volume fraction of gold and silver nanoparticles on the Nusselt number. A diminishing trend in the values of the Nusselt number is noticed with rising values of the volume fraction of nanoparticles (gold and silver). Consequently, the heat transfer rate to the arterial wall diminishes, as heightened volume fractions lead to increased magnitudes of bulk nano-blood temperatures. Ultimately, the overall heat flux to the boundary (arterial wall) is depleted. Also, Au-blood consistently attains significantly higher temperatures than Ag-blood, a consequence of the distinct thermal conductivities of gold and silver nanoparticles. However, there is a decrement in the Nusselt number with the rising arterial curvature parameter, γ , as indicated by the weak decay in profiles. This suggests that with greater arterial wall curvature, the heat transfer rate to the wall diminishes due to reduced contact surface area between the wall and the streaming nano-blood.

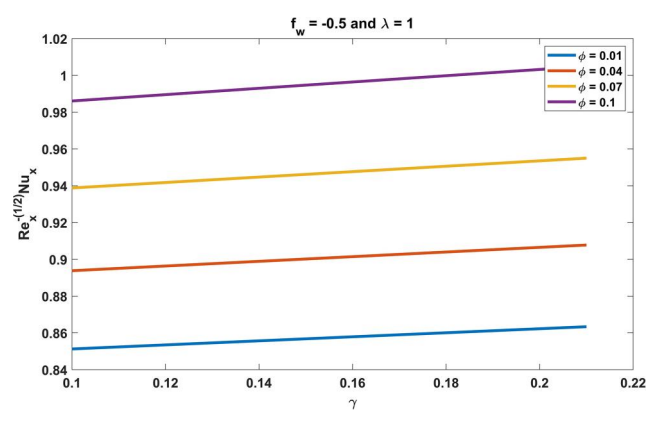


Figure 14. Impact of volume fraction of nanoparticles on Nusselt number coefficient.

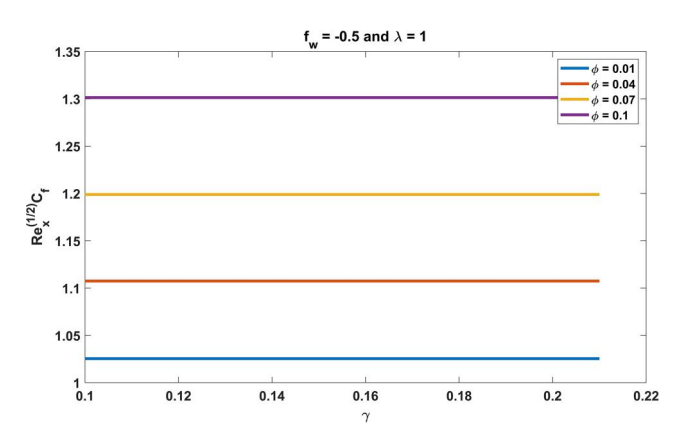


Figure 15. Impact of volume fraction of nanoparticles on skin friction coefficient.

The effect of the volume percentage of gold-blood and silver-blood nanofluids on the arterial wall skin friction coefficient is depicted in Figure 15. It is noteworthy that the skin friction coefficient decreases with increasing volume fraction of nanoparticles. Consequently, higher nanoparticle fusion in the blood induces flow deceleration at the arterial wall boundary. However, the influence on arterial wall skin friction with an increase in the arterial curvature parameter γ is relatively weaker.

Both the Nusselt number and arterial wall skin friction coefficient are pivotal in comprehending fluid flow characteristics and heat transfer in stenotic conditions. These parameters offer valuable insights into the effects of vessel geometry changes on heat transfer processes, crucial for medical diagnostics and treatment planning. The alterations in the skin friction coefficient could carry clinical implications, such as elevated shear stress in stenosed vessels, which potentially contribute to the progression of cardiovascular diseases. The study of the impacts of Nusselt number and arterial wall skin friction can contribute to the

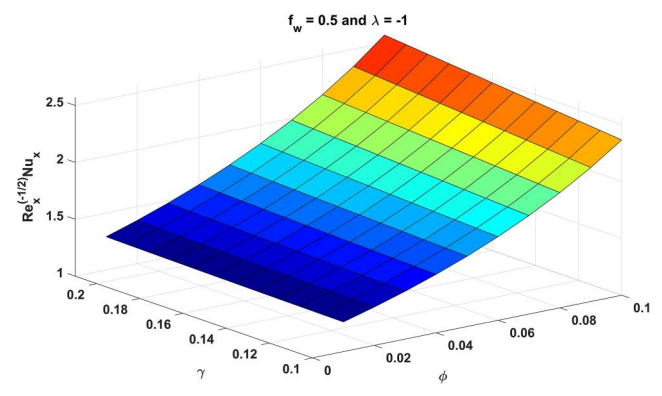


Figure 16. Surface plot for the impact of Nusselt number coefficient (shrinking case).

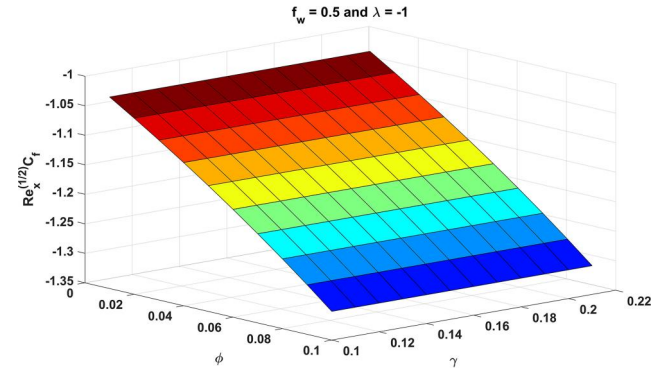


Figure 17. Surface plot for the impact of skin friction coefficient (shrinking case).

treatment of various biomedical conditions ultimately enhancing the quality of patient life.

4.4. Three-dimensional surface plots

Lastly, 3-dimensional surface (contour) plots integrating the impacts of the volume fraction of nanoparticles and flow curvature parameter on the coefficient of skin friction $Re_x^{1/2}C_f$ and Nusselt number $Re_x^{-1/2}Nu_x$ are presented in Figures 16–19. The surface plots corresponding to the shrinking arterial wall case with injection are encapsulated in Figures 16 and 17, while the contour plots corresponding to the stretching arterial wall with suction are explored in Figures 18, Khedher et al. (2023). From these surface plots, it is revealed that the values of skin friction coefficient augment with a larger volume fraction of nanoparticles of Au and Ag while it demonstrates a marginal decline with a rise in the values of the flow parameter. Also, it is clear that the stretching case $\lambda = 1$ and shrinking case $\lambda = -1$ exhibit conflicting behavior. Moreover, the rate of heat convection at the arterial wall (Nusselt number) increases with increasing values of flow curvature parameter for shrinking arterial wall case with injection whereas antagonistic

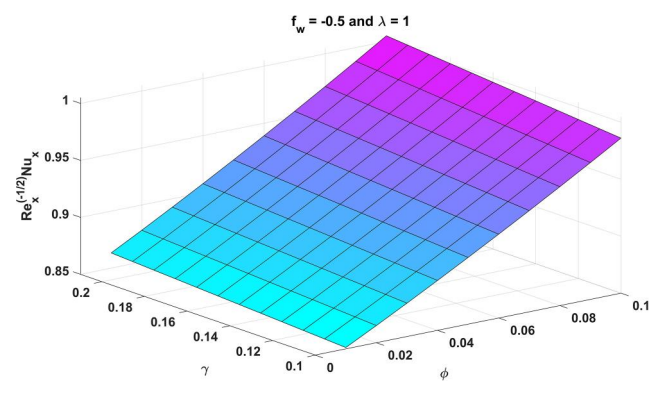


Figure 18. Surface plot for the impact of Nusselt number coefficient (stretching case).

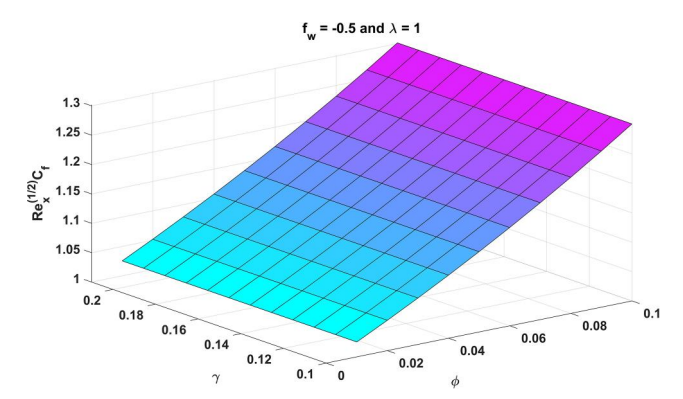


Figure 19. Surface plot for the impact of skin friction coefficient (stretching case).

behavior arises for stretching arterial wall case with suction. Thus an intricate interplay emerges between the mass flux within the arterial wall (suction/injection) and the stretching/shrinking dynamics of the arterial wall, subsequently yielding diverse impacts on the characteristics of skin friction and Nusselt number.

4.5. Numerical results and validation of current nano-blood model

The changes in various pertinent parameters can have a significant impact on the coefficients of heat transfer, such as the Nusselt number, and arterial wall skin friction. The parameters such as magnetic parameter, flow curvature parameter, permeability parameter, thermal radiation parameter, Biot number, and Prandtl number play crucial roles in determining the heat transfer characteristics and flow behavior within arteries. The variations in the magnetic parameter can alter the flow dynamics in magnetohydrodynamic (MHD) flows, affecting both heat transfer and skin friction. Similarly, changes in the permeability parameter can influence fluid flow through porous arterial walls, leading to adjustments in heat transfer and skin friction coefficients. Moreover, adjustments in thermal

Table 4. Numerical values of coefficient of arterial wall skin friction and Nusselt number for varying values of different parameters.

М	γ	β	Rd	Bi	Pr	$Re_x^{-1/2}Nu_x$	$Re_x^{1/2}C_f$
1						2.135724	1.783672
2						1.918572	1.273167
3						1.570398	0.845219
	1					1.912567	1.294594
	2					1.526904	1.458325
	3					1.173893	1.689412
		0.1				1.229273	0.964521
		0.3				1.613879	1.376214
		0.5				1.976801	1.731569
			1			1.037256	1.789132
			2			2.209169	1.432765
			3			3.525737	1.019161
				1		0.946357	1.721964
				2		1.475901	1.432108
				3		1.892167	1.116432
					2	1.172731	2.032156
					4	1.721567	1.837591
					6	2.137598	1.446728

radiation parameters can impact heat transfer mechanisms, consequently affecting the Nusselt number. Determining the numerical values of these coefficients provides valuable insights into the underlying physics of arterial flow and heat transfer phenomena. Table 4 offers a comprehensive compilation of numerical values of the Nusselt number and coefficient of arterial wall skin friction for varying magnetic parameters, flow curvature parameters, permeability parameters, thermal radiation parameters, Biot number, and Prandtl numbers. The analysis of this table enables researchers to understand how the changes in these parameters affect heat transfer and frictional properties within arteries, thereby facilitating the optimization of various biomedical and engineering applications, including cardiovascular device design and thermal therapy planning.

To ascertain the accuracy of the current MATLAB computational code, a benchmarking exercise is conducted against previous solutions presented by Sarwar and Hussain (2021) and Waqas et al. (2022). This comparison is carried out under specific conditions, including the absence of the Sisko material parameter (S = 0), suction/injection parameter $(f_w = 0)$, the volume fraction of nanoparticles ($\phi = 0$), Biot number (Bi = 0), and porosity parameter $(\beta = 0)$ with Sarwar and Hussain (2021) and Waqas et al. (2022). The values of the Nusselt number and Skin friction coefficient are then meticulously compared, as documented in Tables 5 and 6. Notably, the results obtained through the current MATLAB simulations exhibit a remarkable agreement with those reported by Sarwar and Hussain (2021) and Waqas et al. (2022). This alignment between these sets of results instills a high level of confidence in the accuracy and reliability of the present MATLAB solutions.

Table 5. Comparison of Nusselt number with that of Sarwar and Hussain (2021) and Waqas et al. (2022) for $f_w = 0$, Bi = 0, Rd = 1, $\phi_2 = 0$, $\lambda = 1$.

		Current results	Sarwar and Hussain (2021)	Waqas et al. (2022)
ϕ_1	γ	$-k_{nf}/k_{f}\theta^{'}(0)$	$-k_{nf}/k_{f}\theta^{'}(0)$	$-k_{nf}/k_{f}\theta^{'}(0)$
0.01	0.1	2354.342	2358.666	2358.666
0.01	0.12	2280.421	2282.713	2282.713
0.01	0.14	2211.868	2214.476	2214.476
0.05	0.1	2023.312	2025.262	2025.262
0.1	0.1	1760.479	1759.220	1759.220

Table 6. Comparison of skin friction coefficient with that of Sarwar and Hussain (2021) and Waqas et al. (2022) for $f_w = 0$, Bi = 0, Rd = 1, $\phi_2 = 0$, $\lambda = 1$.

		Current results	Sarwar and Hussain (2021)	Waqas et al. (2022)
ϕ_1	γ	$-1/2C_fRe$	$-1/2C_fRe$	$-1/2C_fRe$
0.01	0.1	0.934732	0.939968	0.939968
0.01	0.12	0.929461	0.924794	0.924794
0.01	0.14	0.918213	0.911311	0.911311
0.05	0.1	1.323572	1.329552	1.329552
0.1	0.1	1.171432	1.175985	1.175985

Table 7. Comparison of Nusselt number values for different nanoparticles.

ϕ	γ	Gold	Silver	Iron oxide	Lipid	Silicon	Magnetic
0.01	0.1	0.754123	0.654392	0.607172	0.607753	0.607619	0.605328
0.01	0.12	0.757638	0.657861	0.608257	0.608891	0.608874	0.606497
0.01	0.14	0.759043	0.659329	0.609351	0.609994	0.609947	0.607549
0.05	0.1	0.815329	0.693837	0.653374	0.655971	0.655982	0.646383
0.1	0.1	0.923568	0.834798	0.750439	0.758208	0.759487	0.7333914

Moreover, the comparative analysis conducted in Table 7 delves into the realm of heat transfer rates, as quantified by the Nusselt number, across nanoparticles exhibiting commendable biocompatibility. This meticulous evaluation is underpinned by the consideration of fixed values for the following key parameters: $M = 1, Pr = 6.2, Rd = 1.2, Bi = 1, f_w = -0.5, \text{ and } \beta =$ 0.1. Within this framework, it emerges that gold and silver nanoparticles eclipse their counterparts in terms of Nusselt number, thus asserting their superiority in facilitating heat transfer phenomena. This discernible advantage can be attributed to the exceptional thermal conductivity inherent in gold and silver nanoparticles. Consequently, the selection of gold and silver nanoparticles is not merely an arbitrary choice but a judicious one, firmly grounded in the empirical evidence presented within the literature.

5. Concluding remarks

The motivation behind the treatment of stenosis lies in the pursuit of advanced therapeutic solutions that leverage cutting-edge technologies. To address this, a

sophisticated nano-blood model incorporating gold and silver nanoparticles has been developed. This model accounts for crucial physiological factors such as the stretching or shrinking of the arterial wall, suction or injection at the arterial boundary, and the presence of a porous arterial wall. Additionally, it considers convective wall heating and the intricate effects of viscous dissipation within the bloodstream. The linked non-linear partial differential expressions of the proposed model are transformed into ODEs (dimensionless) by applying the relevant similarity variables. Higher-order ODEs are then reduced to a first-order system of ODEs which is further solved using the bvp4c solver in MATLAB. Subsequently, numerical results are presented in the form of tables and graphical representations are meticulously analyzed. The main conclusions derived from the current simulations can be delineated as follows:

- An elevation in the volume fraction, arterial curvature parameter, suction parameter, and permeability parameter prompts a reduction in the velocity of both gold-blood and silver-blood nanofluids. Conversely, heightened injection intensity at the arterial wall leads to acceleration.
- 2. The gold-blood nanofluid consistently demonstrates higher velocity magnitudes compared to the silver-blood nanofluid.
- 3. The temperature levels exhibit augmentation with elevations in the volume fraction of gold or silver nanoparticles and the curvature parameter.
- The elevated temperatures are computed for the stretching sheet case and gold-blood nanofluid in comparison to the shrinking sheet case and silver-blood nanofluid.
- 5. The temperature experiences a reduction as the thermal Biot number, representing the convective cooling parameter at the arterial wall, increases. This decrement is due to the presence of viscous dissipation, wherein mechanical energy is transformed into heat within the nanofluid.
- A declining trend in the values of the skin friction coefficient is observed alongside an increasing trend in the volume fraction.
- 7. A reduction in the Nusselt number values is observed with an increase in the volume fraction of nanoparticles. This phenomenon arises from the heightened doping of the blood with nanoparticles, leading to increased heating within the bulk fluid. Consequently, there is a decrease in heat flux to the arterial wall. The presence of porous walls further contributes to this effect, as it

- alters the heat transfer dynamics and impedes the heat flux from the nanofluids to the arterial wall.
- The Nusselt number experiences an increase with a rise in the curvature parameter for the shrinking arterial wall case with injection, whereas it undergoes a decrease for the stretching arterial wall case with suction.

Nomenclature

Bi	Biot number (-)
Ср	Heat transfer coefficient (Jkg ⁻¹ K ⁻¹)
f_w	Suction/Injection parameter (-)
K	Permeability coefficient (-)
k	Thermal conductivity coefficient (Blood) (W m ⁻¹
	K^{-1})
M	Magnetic flux parameter (-)
Pr	Prandtl number (-)
<i>r</i> , <i>x</i>	Spatial coordinates axis (m)
Rd	Thermal radiation parameter (-)
T	Temperature (K)
<i>u</i> , <i>v</i>	Projections of velocity vector (ms ⁻¹)

Greek Letter

β	Porosity parameter (-)
γ	Flow curvature parameter (-)
ϕ	Nanoparticle Volume fraction (-)
η	Free variable (-)
μ	Absolute viscosity of blood (kgms ⁻¹)
ν	Momentum diffusivity of blood (Ns ⁻²)
ρ	Density of blood (kg m ⁻³)
ρ Ср	Specific heat capacity of blood

Subscripts

f	Blood
S	Solid Nanoparticles
nf	Nanofluid
w	At wall
∞	Free-Stream

Acknowledgments

The authors express their gratitude for the unconditional support received from Universiti Teknikal Malaysia Melaka.

Disclosure statement

The authors declare that they have no known competing financial interests or personal relationships that could have appeared to influence the work reported in this article.

Funding

The funding for this project has been provided by the Fundamental Research Grant Scheme (FRGS/1/2024/ STG06/UTEM/03/1) awarded by Ministry of Higher Education, Malaysia.

References

- Aarathy RA, Gopika SM, Savitha Pillai S. 2020. Recent insights into the potential of magnetic metal nanostructures as magnetic hyperthermia agents. Sens Lett. 18(12): 861-880. doi: 10.1166/sl.2020.4297.
- Abid N, Hasnain J. 2024. Viscous dissipation effects on the axisymmetric flow of Casson rheological fluid in the core region of curved artery surrounded by Al₂O₃/γ-Al₂O₃ nanofluid. Int J Heat Fluid Flow. 107:109349. doi: 10. 1016/j.ijheatfluidflow.2024.109349.
- Abumandour R, Eldesoky IM, Abumandour M, Morsy K, Ahmed MM. 2022. Magnetic field effects on thermal nanofluid flowing through vertical stenotic artery: analytical study. Mathematics. 10(3):492. doi: 10.3390/ math10030492.
- Agyare E, Kandimalla K. 2014. Delivery of polymeric nanoparticles to target vascular diseases. J Biomol Res Ther. 3(1):S1-S001. doi: 10.4172/2167-7956.s1-001.
- Ahamed M, Khan MM, Siddiqui M, AlSalhi MS, Alrokayan SA. 2011. Green synthesis, characterization and evaluation of biocompatibility of silver nanoparticles. Physica E. 43(6):1266-1271. doi: 10.1016/j.physe.2011.02.014.
- Ahmed A, Nadeem S. 2016. The study of (Cu, TiO2, Al2O3) nanoparticles as antimicrobials of blood flow through diseased arteries. J Mol Liq. 216:615-623. doi: 10.1016/j.molliq.2016.01.059.
- Akbar NS. 2015. Carbon nano tubes analysis for blood flow in stenosed tapered arteries. IEEE Trans Nanotechnol. 14(3):452-463. doi: 10.1109/TNANO.2015.2406337.
- Akhlaghi S, Rabbani S, Alavi S, Alinaghi A, Radfar F, Dadashzadeh S, Haeri A. 2019. Green formulation of curcumin loaded lipid-based nanoparticles as a novel carrier for inhibition of post-angioplasty restenosis. Mater Sci Eng C Mater Biol Appl. 105:110037. doi: 10.1016/j. msec.2019.110037.
- Alharbi KAM, Ali J, Ramzan M, Kadry S, Saeed AM. 2024. A comarative analysis of hybrid nanofluid flow through an electrically conducting vertical microchannel using Yamada-Ota and Xue models. Numer Heat Transf A. 85(9):1501-1516. doi: 10.1080/10407782.2023.2205183.
- Alhussain ZA. 2022. A comprehensive study of thermal conductivity models with metallic and non-metallic nanoparticles in the blood flow through a regular catheter in multi-stenosed artery. Appl Nanosci. 12(12):4033-4045. doi: 10.1007/s13204-022-02622-3.
- Ansari K, Ahmad R, Tanweer MS, Azam I. 2024. Magnetic iron oxide nanoparticles as a tool for the advancement of biomedical and environmental application: a review. Biomed Mater Devices. 2(1):139-157. doi: 10.1007/ s44174-023-00091-y.
- Arabestani MR, Bigham A, Kamarehei F, Dini M, Gorjikhah F, Shariati A, Hosseini SM. 2024. Solid lipid nanoparticles and their application in the treatment of bacterial infectious diseases. Biomed Pharmacother. 174: 116433. doi: 10.1016/j.biopha.2024.116433.
- Arshad F, Naikoo GA, Hassan IU, Chava SR, El-Tanani M, Aljabali AA, Tambuwala MM. 2024. Bioinspired and green synthesis of silver nanoparticles for medical applications: a green perspective. Appl Biochem Biotechnol. 196(6):3636-3669. doi: 10.1007/s12010-023-04719-z.

- Asefa T, Tao Z. 2012. Biocompatibility of mesoporous silica nanoparticles. Chem Res Toxicol. 25(11):2265-2284. doi: 10.1021/tx300166u.
- Ashwini T, Narayan R, Shenoy PA, Nayak UY. 2022. Computational modeling for the design and development of nano based drug delivery systems. J Mol Liq. 368: 120596. doi: 10.1016/j.molliq.2022.120596.
- Austin LA, Mackey MA, Dreaden EC, El-Sayed MA. 2014. The optical, photothermal, and facile surface chemical properties of gold and silver nanoparticles in biodiagnostics, therapy, and drug delivery. Arch Toxicol. 88(7): 1391-1417. doi: 10.1007/s00204-014-1245-3.
- Badfar H, Yekani Motlagh S, Sharifi A. 2020. Numerical simulation of magnetic drug targeting to the stenosis vessel using Fe₃O₄ magnetic nanoparticles under the effect of magnetic field of wire. Cardiovasc Eng Technol. 11(2): 162-175. doi: 10.1007/s13239-019-00446-x.
- Barman A. 2015. Review on biocompatibility of ZnO nano particles. In Advancements of medical electronics: proceedings of the first international conference, ICAME 2015; New Delhi: Springer. p. 343-352.
- Beliaev AY, Kozlov SM. 1996. Darcy equation for random porous media. Comm Pure Appl Math. 49(1):1-34. doi: 10.1002/ (SICI)1097-0312(199601)49;1<1::AID-CPA1>3.0.CO;2-J.
- Bhatti MM, Sait SM, Ellahi R. 2022. Magnetic nanoparticles for drug delivery through tapered stenosed artery with blood based non-Newtonian fluid. Pharmaceuticals. 15(11):1352. doi: 10.3390/ph15111352.
- Bian Y, Jin Q, He J, Ngo T, Bae O-N, Pi J, Chung HY, Xu Y. 2023. Exposure to titanium dioxide nanoparticles increases trisk of arterial thrombosis: involvement of calcium-dependent platelet aggregation and procoagulant activity.
- Boujelbene M, Rehman S, Alqahtani S, Alshehery S. 2023. Second law assessment of injected nanoparticles to blood flow with thermal radiation and magnetic field in conduit artery. J Taiwan Inst Chem Eng. 150:105074. doi: 10.1016/j.jtice.2023.105074.
- Boujelbene M, Rehman S, Balegh M, Hashim. 2025. Entropy degradation in a dual diffusion flow of a non-Newtonian fluid in inclined channel using Keller-box approach. Math Methods App Sci. 48(7):8342-8368. doi: 10.1002/mma.9843.
- Chan JM, Rhee J-W, Drum CL, Bronson RT, Golomb G, Langer R, Farokhzad OC. 2011. In vivo prevention of arterial restenosis with paclitaxel-encapsulated targeted lipid-polymeric nanoparticles. Proc Natl Acad Sci USA. 108(48):19347-19352. doi: 10.1073/pnas.1115945108.
- Cheng L, Bandarra Filho EP, Thome JR. 2008. Nanofluid two-phase flow and thermal physics: a new research frontier of nanotechnology and its challenges. J Nanosci Nanotechnol. 8(7):3315-3332. doi: 10.1166/jnn.2008.413.
- Chłopek J, Czajkowska B, Szaraniec B, Frackowiak E, Szostak K, Béguin F. 2006. In vitro studies of carbon nanotubes biocompatibility. Carbon. 44(6):1106-1111. doi: 10.1016/j.carbon.2005.11.022.
- Cinar Y, Enyol AMS, Duman K. 2001. Blood viscosity and blood pressure: role of temperature and hyperglycemia. Am J Hyper Tension. 14(5):433-438. doi: 10.1016/S0895-7061(00)01260-7.
- Connor EE, Mwamuka J, Gole A, Murphy CJ, Wyatt MD. 2005. Gold nanoparticles are taken up by human cells

- but do not cause acute cytotoxicity. Small. 1(3):325-327. doi: 10.1002/smll.200400093.
- Dabagh M, Jalali P, Tarbell JM. 2009. The transport of LDL across the deformable arterial wall: the effect of endothelial cell turnover and intimal deformation under hypertension. Am J Physiol Heart Circ Physiol. 297(3):H983-H996. doi: 10.1152/ajpheart.00324.2009.
- Das S, Karmakar P, Ali A. 2022. Electrothermal blood streaming conveying hybridized nanoparticles in a nonuniform endoscopic conduit. Med Biol Eng Comput. 60(11):3125-3151. doi: 10.1007/s11517-022-02650-9.
- Dhayalan M, Wang W, Riyaz SM, Dinesh RA, Shanmugam J, Irudayaraj SS, Stalin A, Giri J, Mallik S, Hu R. 2024. Advances in functional lipid nanoparticles: from drug delivery platforms to clinical applications. 3 Biotech. 14(2):57. doi: 10.1007/s13205-023-03901-8.
- Elhanafy A, Abuouf Y, Elsagheer S, Ookawara S, Ahmed M. 2023. Effect of external magnetic field on realistic bifurcated right coronary artery hemodynamics. Phys Fluids. 35(6):061903. doi: 10.1063/5.0152322.
- Encinas-Basurto D, Eedara BB, Mansour HM. 2024. Biocompatible biodegradable polymeric nanocarriers in dry powder inhalers (DPIs) for pulmonary inhalation delivery. J Pharm Investig. 54(2):145-160. doi: 10.1007/ s40005-024-00671-0.
- Fahim M, Sajid M, Ali N. 2024. Pulsatile pressure-driven non-Newtonian blood flow through a porous stenotic artery: a computational analysis. Numer Heat Transf A. :1-21. doi: 10.1080/10407782.2024.2326961.
- Fangfang F, Sajid T, Jamshed W, Eid MR, Altamirano GC, Altaf I, Abd-Elmonem A, El Din SM. 2023. Thermal transport and characterized flow of trihybridity Tiwari and Das Sisko nanofluid via a stenosis artery: a case study. Case Stud Therm Eng. 47:103064. doi: 10.1016/j. csite.2023.103064.
- Geszke-Moritz M, Moritz M. 2024. Biodegradable polymeric nanoparticle-based drug delivery systems: comprehensive overview, perspectives and challenges. Polymers. 16(17):2536. doi: 10.3390/polym16172536.
- Ghazal H, Waqar A, Yaseen F, Shahid M, Sultana M, Tariq M, Bashir MK, Tahseen H, Raza T, Ahmad F. 2024. Role of nanoparticles in enhancing chemotherapy efficacy for cancer treatment. Next Mater. 2:100128. doi: 10.1016/j. nxmate.2024.100128.
- Gomes HIO, Martins CSM, Prior JAV. 2021. Silver nanoparticles as carriers of anticancer drugs for efficient target treatment of cancer cells. Nanomaterials. 11(4):964. doi: 10.3390/nano11040964.
- Govindarajulu K, Subramanyam Reddy A. Magnetohydrodynamic pulsatile flow of third grade hybrid nanofluid in a porous channel with Ohmic heating and thermal radiation effects. Phys Fluids. 34(1): 013105. doi: 10.1063/5.0074894.
- Guillemot F, Souquet A, Catros S, Guillotin B. 2010. Laserassisted cell printing: principle, physical parameters versus cell fate and perspectives in tissue engineering. Nanomedicine. 5(3):507-515. doi: 10.2217/nnm.10.14.
- Gul A, Tzirtzilakis EE, Makhanov SS. 2022. Simulation of targeted magnetic drug delivery: two-way coupled biomagnetic fluid dynamics approach. Phys Fluids. 34(2): 021911. doi: 10.1063/5.0080216.



- Gupta D, Roy P, Sharma R, Kasana R, Rathore P, Gupta TK. 2024. Recent nanotheranostic approaches in cancer research. Clin Exp Med. 24(1):8. doi: 10.1007/s10238-023-01262-3.
- Hanche-Olsen H. 2004. Buckingham's pi-theorem. NTNU. http://www.math.ntnu.no/hanche/notes/buckingham/ buckingham-a4.pdf.
- Hashemzadeh S, Bina F, Khounsari HM, Hashemzadeh S. 2024. Nanotechnology in the development of cardiac stents. J Drug Delivery Sci Technol. 95:105596. doi: 10. 1016/j.jddst.2024.105596.
- He X, Ni X, Wang Y, Wang K, Jian L. 2011. Electrochemical detection of nicotinamide adenine dinucleotide based on molecular beacon-like DNA and E. coli DNA ligase. Talanta. 83(3):937-942. doi: 10.1016/ i.talanta.2010.10.051.
- Hirsch LR, Stafford RJ, Bankson J, Sershen SR, Rivera B, Price R, Hazle JD, Halas NJ, West JL. 2003. Nanoshellmediated near-infrared thermal therapy of tumors under magnetic resonance guidance. Proc Natl Acad Sci USA. 100(23):13549-13554. doi: 10.1073/pnas.2232479100.
- Huang Y, Guo X, Wu Y, Chen X, Feng L, Xie N, Shen G. 2024. Nanotechnology's frontier in combatting infectious and inflammatory diseases: prevention and treatment. Signal Transduct Target Ther. 9(1):34. doi: 10.1038/s41392-024-01745-z.
- Humphrey JD. 1995. Mechanics of the arterial wall: review and directions. Crit Rev Biomed Eng. 23(1-2):1-162.
- Hussain A, Riaz Dar MN, Khalid Cheema W, Kanwal R, Han Y. 2024. Investigating hybrid nanoparticles for drug delivery in multi-stenosed catheterized arteries under magnetic field effects. Sci Rep. 14(1):1170. doi: 10.1038/ s41598-024-51607-5.
- Hussain A, Sarwar L, Rehman A, Akbar S, Gamaoun F, Coban HH, Almaliki AH, Alqurashi MS. 2022. Heat transfer analysis and effects of (silver and gold) nanoparticles on blood flow inside arterial stenosis. Appl Sci. 12(3):1601. doi: 10.3390/app12031601.
- Islam P, Schaly S, Abosalha AK, Boyajian J, Thareja R, Ahmad W, Shum-Tim D, Prakash S. 2024. Nanotechnology in development of next generation of stent and related medical devices: current and future aspects. Wiley Interdiscip Rev Nanomed Nanobiotechnol. 16:e1941.
- Kadhim RJ, Karsh EH, Taqi ZJ, Jabir MS. 2021. Biocompatibility of gold nanoparticles: in-vitro and invivo study. Mater Today: Proc. 42:3041-3045. doi: 10. 1016/j.matpr.2020.12.826.
- Kalashgrani MY, Mousavi SM, Akmal MH, Gholami A, Omidifar N, Chiang W-H, Althomali RH, Lai CW, Rahman MM. 2024. Gold fluorescence nanoparticles for enhanced SERS detection in biomedical sensor applications: current trends and future directions. Chem Rec. :e202300303. doi: 10.1002/tcr.202300303.
- Khaled A-R, Vafai K. 2003. The role of porous media in modeling flow and heat transfer in biological tissues. Int J Heat Mass Transf. 46(26):4989-5003. doi: 10.1016/ S0017-9310(03)00301-6.
- Khalifehzadeh R, Arami H. 2020. Biodegradable calcium phosphate nanoparticles for cancer therapy. Adv Colloid Interface Sci. 279:102157. doi: 10.1016/j.cis.2020.102157.
- Khanduri U, Sharma BK, Sharma M, Mishra NK, Saleem 2023. Sensitivity analysis of electroosmotic

- magnetohydrodynamics fluid flow through the curved stenosis artery with thrombosis by response surface optimization. Alex Eng J. 75:1-27. doi: 10.1016/j.aej.2023.05.
- Khanduri U, Sharma BK. 2023. Hall and ion slip effects on hybrid nanoparticles (au-go/blood) flow through a catheterized stenosed artery with thrombosis. Proc Inst Mech Eng C. 237:2256-2278.
- Kharlamov AN, Tyurnina AE, Veselova VS, Kovtun OP, Shur VY, Gabinsky JL. 2015. Silica-gold nanoparticles for atheroprotective management of plaques: results of the nanom-fim trial. Nanoscale. 7(17):8003-8015. doi: 10. 1039/c5nr01050k.
- Khedher NB, Rehman S, Algahtani S, Alshehery S, Hashim. 2023. Comparative study of entropy distribution for generalized fluid between an inclined channel in the perspective of classical and non-Fourier's law. Eng Sci Technol Int J. 45:101471. doi: 10.1016/j.jestch.2023.101471.
- King M, Gee D. 2010. Multiscale modeling of particle interactions: applications in biology and nanotechnology. USA: John Wiley & Sons.
- Kozlov N, Volchkov S, Blyakhman F, Chestukhin V, Kurlyand-Skaya G. 2022. The modeling of magnetic detection of iron oxide nanoparticles in the stream of patient-specific artery with stenotic lesion: the effects of vessel geometry and particle concentration. IEEE Trans Magn. 58(8):1-5. doi: 10.1109/TMAG.2022.3162884.
- Kus-Liśkiewicz M, Fickers P, Ben Tahar I. 2021. Biocompatibility and cytotoxicity of gold nanoparticles: recent advances in methodologies and regulations. Int J Mol Sci. 22(20):10952. doi: 10.3390/ijms222010952.
- Lan Z, Lyu Y, Xiao J, Zheng X, He S, Feng G, Zhang Y, Wang S, Kislauskis E, Chen J, et al. 2014. Novel biodegradable drug-eluting stent composed of poly-l-lactic acid and amorphous calcium phosphate nanoparticles demonstrates improved structural and functional performance for coronary artery disease. J Biomed Nanotechnol. 10(7):1194-1204. doi: 10.1166/jbn.2014.1868.
- Langhaar HL. 1951. Dimensional analysis and theory of models. USA: Wiley.
- Li Z, Jiao D, Zhang W, Ren K, Qiu L, Tian C, Li Y, Li J, Zhou X, Zhao Y, et al. 2021. Antibacterial and antihyperplasia polylactic acid/silver nanoparticles nanofiber membrane-coated airway stent for tracheal stenosis. Colloids Surf B Biointerfaces. 206:111949. doi: 10.1016/j.colsurfb. 2021.111949.
- Li Z, Tian C, Jiao D, Li J, Li Y, Zhou X, Zhao H, Zhao Y, Han X. 2022. Synergistic effects of silver nanoparticles and cisplatin in combating inflammation and hyperplasia of airway stents. Bioact Mater. 9:266-280. doi: 10.1016/j. bioactmat.2021.07.029.
- Liu Y, Tan J, Thomas A, Ou-Yang D, Muzykantov VR. 2012. The shape of things to come: importance of design in nanotechnology for drug delivery. Ther Deliv. 3(2): 181-194. doi: 10.4155/tde.11.156.
- Lund LA, Yashkun U, Shah NA. 2023. Magnetohydrodynamics streamwise and cross flow of hybrid nanofluid along the viscous dissipation effect: duality and stability. Phys Fluids. 35(2):023320. doi: 10.1063/5.0135361.
- Mahalakshmi S, Hema N, Vijaya PP. 2020. In vitro biocompatibility and antimicrobial activities of zinc oxide nanoparticles (ZnO NPs) prepared by chemical and green

- synthetic route—a comparative study. BioNanoSci. 10(1): 112-121. doi: 10.1007/s12668-019-00698-w.
- Majee S, Shit G. 2020. Modeling and simulation of blood flow with magnetic nanoparticles as carrier for targeted drug delivery in the stenosed artery. Eur J Mech B. 83: 42-57. doi: 10.1016/j.euromechflu.2020.04.004.
- Markides H, Rotherham M, El Haj A. Biocompatibility and toxicity of magnetic nanoparticles in regenerative medicine. J Nanomater. 2012(1):614094. doi: 10.1155/2012/614094.
- Mashiku LR, Shaw S. 2023. Unsteady nano-magnetic drug dispersion for pulsatile Darcy flow through microvessel with drug elimination phenomena. Phys Fluids. 35(10): 101909. doi: 10.1063/5.0171286.
- Mishra NK. 2024. Computer simulation of heat and mass transfer effects on nanofluid flow of blood through an inclined stenosed artery with hall effect. Acta Mech Autom. 18(1):129-138. doi: 10.2478/ama-2024-0017.
- Nadeem S, Ijaz S. 2015. Single wall carbon nanotube (SWCNT) examination on blood flow through a multiple stenosed artery with variable nanofluid viscosity. AIP Adv. 5(10):107217. doi: 10.1063/1.4934583.
- Nicol JR, Dixon D, Coulter JA. 2015. Gold nanoparticle surface functionalization: a necessary requirement in the development of novel nan-otherapeutics. Nanomedicine. 10(8):1315-1326. doi: 10.2217/nnm.14.219.
- Omama M, Arafa AA, Elsaid A, Zahra WK. 2024. MHD flow of the novel quadruple hybrid nanofluid model in a stenosis artery with porous walls and thermal radiation: a Sisko model-based analysis. J Appl Math Mech. 104(6): e202300719.
- Painter PR, Edén P, Bengtsson H-U. 2006. Pulsatile blood flow, shear force, energy dissipation and Murray's law. Theor Biol Med Modell. 3:1-10. doi: 10.1186/1742-4682-3-31.
- Patankar S. 2018. Numerical heat transfer and fluid flow. Boca Raton: CRC Press.
- Prasad B, Bali R. 2023. Mathematical study of nanoparticle loaded in red blood cells for drug delivery in an artery with stenosis. Phys Fluids. 35(9):091902. doi: 10.1063/5. 0167245.
- Raju C, Basha HT, Noor N, Shah NA, Yook S-J. 2024. Significance of body acceleration and gold nanoparticles through blood flow in an uneven/composite inclined stenosis artery: a finite difference computation. Math Comput Simul. 215:399-419. doi: 10.1016/j.matcom.2023.08.006.
- Rashid MM, Forte Tavčer P, Tomšič B. 2021. Influence of titanium dioxide nanoparticles on human health and the environment. Nanomaterials. 11(9):2354. doi: 10.3390/ nano11092354.
- Ratha P, Tripathy R, Mishra S. 2023. Particle-shape illustration via the Hamilton-Crosser and Yamada-Ota hybrid nanofluid flow models past a stretching cylinder. Eur Phys J Plus. 138(2):1-15. doi: 10.1140/epjp/s13360-023-03752-5.
- Reddy LH, Arias JL, Nicolas J, Couvreur P. 2012. Magnetic nanoparticles: design and characterization, toxicity and biocompatibility, pharmaceutical and biomedical applications. Chem Rev. 112(11):5818-5878. doi: 10.1021/cr300068p.
- Rehman S, Trabelsi Y, Alqahtani S, Alshehery S, Eldin SM, Hashim. 2023. A renovated Jaffrey-Hamel flow problem and new scaling statistics for heat, mass fluxes with Cattaneo-Christov heat flux model. Case Stud Therm Eng. 43:102787. doi: 10.1016/j.csite.2023.102787.

- Rehman S, Alfaleh A, Afef K, Ali Shah SI, Hashim. 2023. Onset about isothermal flow of Carreau liquid over converging channel with Cattaneo-Christov heat and mass fluxes. Heliyon. 9(5):e15710. doi: 10.1016/j.heliyon.2023. e15710.
- Rehman S, Alqahtani S, Alshehery S, Boujelbene M, Hashim. 2023. Modelling heat-mass transport for mhd eyring-Powell hybrid nanofluid over an expanding surface laden by autocatalytic chemical reaction and nanoparticles diffusion. Adv Eng Softw. 186:103549. doi: 10. 1016/j.advengsoft.2023.103549.
- Sajid T, Gari AA, Jamshed W, Eid MR, Islam N, Irshad K, Altamirano GC, El Din SM. 2023. Case study of autocatalysis reactions on tetra hybrid binary nanofluid flow via Riga wedge: biofuel thermal application. Case Stud Therm Eng. 47:103058. doi: 10.1016/j.csite.2023.103058.
- Sajid T, Jamshed W, Eid MR, Altamirano GC, Aslam F, Alanzi AM, Abd-Elmonem A. 2023. Magnetized cross tetra hybrid nanofluid passed a stenosed artery with nonuniform heat source (sink) and thermal radiation: novel tetra hybrid Tiwari and Das nanofluid model. J Magn Magn Mater. 569: 170443. doi: 10.1016/j.jmmm.2023.170443.
- Sarwar L, Hussain A, Fernandez-Gamiz U, Akbar S, Rehman A, Sherif E-SM. 2022. Thermal enhancement and numerical solution of blood nanofluid flow through stenotic artery. Sci Rep. 12(1):17419. doi: 10.1038/ s41598-022-20267-8.
- Sarwar L, Hussain A. 2021. Flow characteristics of au-blood nanofluid in stenotic artery. Int Commun Heat Mass Transfer. 127:105486. doi: 10.1016/j.icheatmasstransfer. 2021.105486.
- Schneider MGM, Lassalle VL. 2017. Magnetic iron oxide nanoparticles as novel and efficient tools for atherosclerosis diagnosis. Biomed Pharmacother. 93:1098-1115. doi: 10.1016/j.biopha.2017.07.012.
- Shabbir R, Raza A, Liaquat A, Shah SU, Saeed S, Sarwar U, Hamza M, Chudhary F, Hussain Z, Butt N. 2022. Nanoparticles as a novel tool to inhibit inflammatory cytokines in human lymphocytes and macrophages of coronary artery disease. J Pharm Sci. 111(5):1509-1521. doi: 10.1016/j.xphs.2022.01.001.
- Shahbazi M-A, Hamidi M, Mäkilä EM, Zhang H, Almeida PV, Kaasalainen M, Salonen JJ, Hirvonen JT, Santos HA. 2013. The mechanisms of surface chemistry effects of mesoporous silicon nanoparticles on immunotoxicity and biocompatibility. Biomaterials. 34(31):7776-7789. doi: 10. 1016/j.biomaterials.2013.06.052.
- Shahzad MH, Awan AU, Guedri K, Fadhl BM, Oreijah M. 2024. Entropy-based investigation of blood flow in elliptical multi-stenotic artery with hybrid nanofluid in a fuzzy environment: applications as drug carriers for brain diseases. Eng Appl Artif Intell. 130:107695. doi: 10.1016/ j.engappai.2023.107695.
- Shi W, Fuad ARM, Li Y, Wang Y, Huang J, Du R, Wang G, Wang Y, Yin T. 2023. Biodegradable polymeric nanoparticles increase risk of cardiovascular diseases by inducing endothelium dysfunction and inflammation. J Nanobiotechnology. 21(1):65. doi: 10.1186/s12951-023-01808-3.
- Shiozaki AA, Senra T, Morikawa AT, Deus DF, Paladino-Filho AT, Pinto IM, Maranhão RC. 2016. Treatment of patients with aortic atherosclerotic disease



- paclitaxel-associated lipid nanoparticles. Clinics. 71(8): 435-439. doi: 10.6061/clinics/2016(08)05.
- Smart S, Cassady A, Lu G, Martin D. 2006. The biocompatibility of carbon nanotubes. Carbon. 44(6):1034-1047. doi: 10.1016/j.carbon.2005.10.011.
- Sokolova V, Epple M. 2021. Biological and medical applications of calcium phosphate nanoparticles. Chemistry. 27(27):7471-7488. doi: 10.1002/chem.202005257.
- Song K, Su X, Zhao W, Ai F, Umar A, Baskoutas S. 2024. Functional inorganic nanomaterials for optical cancer theranostics. Chem Eng J. 485:150067. doi: 10.1016/j.cej. 2024.150067.
- Tadić M, Jagličić Z, Lazović J, Nemec S, Kralj S. 2025. Spion clusters with porous silica shell: synthesis, coreshell structure, magnetic properties, biocompatibility and MRI application. Ceram Int. 51(12):15521-15534. doi: 10.1016/j.ceramint.2025.01.388.
- Tang T-Q, Rooman M, Shah Z, Jan MA, Vrinceanu N, Racheriu M. 2023. Computational study and characteristics of magnetized gold-blood Oldroyd-B nanofluid flow and heat transfer in stenosis narrow arteries. J Magn Magn Mater. 569:170448. doi: 10.1016/j.jmmm.2023. 170448.
- Tang T-Q, Rooman M, Vrinceanu N, Shah Z, Alshehri A. 2022. Blood flow of Au-nanofluid using Sisko model in stenotic artery with porous walls and viscous dissipation Micromachines. 13(8):1303. doi: 10.3390/ effect. mi13081303.
- Thakur A, Kumar A. 2024. Strategies for enhancing biocompatibility of nanoparticles. Nanoparticle Tox Compat. 161:182-224.
- Thirumalaisamy K, Ramachandran S, Ramachandra Prasad V, Anwar Bég O, Leung H-H, Kamalov F, Panneer Selvam R. 2022. Comparative heat transfer analysis of electroconductive Fe3O4-MWCNT-water and Fe3O4-MWCNT-kerosene hybrid nanofluids in a square porous cavity using the non-Fourier heat flux model. Phys Fluids. 34(12):122016. doi: 10.1063/5.0127463.
- Tiwari RK, Das MK. 2007. Heat transfer augmentation in a two-sided lid-driven differentially heated square cavity utilizing nanofluids. Int J Heat Mass Transf. 50(9-10): 2002-2018. doi: 10.1016/j.ijheatmasstransfer.2006.09.034.
- Tripathi J, Vasu B, Bég OA, Gorla RSR. 2021. Unsteady hybrid nanoparticle-mediated magneto-hemodynamics and heat transfer through an overlapped stenotic artery: biomedical drug delivery simulation. Proceedings of the Institution of Mechanical Engineers, Part H: Journal of Engineering in Medicine (vol. 235). p. 1175-1196.
- Tripathi J, Vasu B, Subba Reddy Gorla R, Chamkha AJ, Murthy PVSN, Anwar Bég O. 2021. Blood flow mediated hybrid nanoparticles in human arterial system: recent research, development and applications. J Nanofluids. 10(1):1-30. doi: 10.1166/jon.2021.1769.
- Tzirtzilakis E. 2005. A mathematical model for blood flow in magnetic field. Phys Fluids. 17(7):077103. doi: 10. 1063/1.1978807.
- Varmazyar M, Habibi M, Amini M, Pordanjani AH, Afrand M, Vahedi SM. 2020. Numerical simulation of

- magnetic nanoparticle-based drug delivery in presence of atherosclerotic plaques and under the effects of magnetic field. Powder Technol. 366:164-174. doi: 10.1016/j.powtec.2020.02.009.
- Vedernikova I. 2015. Magnetic nanoparticles: advantages of using, methods for preparation, characterization, application in pharmacy. Ref J Chem. 5(3):256-280. doi: 10. 1134/S2079978015030036.
- Verma R. 2018. Analysis and simulation of nano fluids flow using matlab. India: National Institute of Technology.
- Wang S, He H, Mao Y, Zhang Y, Gu N. 2024. Advances in atherosclerosis theranostics harnessing iron oxide-based nanoparticles. Adv Sci. 11(17):2308298. doi: 10.1002/ advs.202308298.
- Waqas H, Farooq U, Hassan A, Liu D, Noreen S, Makki R, Imran M, Ali MR. 2023. Numerical and computational simulation of blood flow on hybrid nanofluid with heat transfer through a stenotic artery: silver and gold nanoparticles. Results Phys. 44:106152. doi: 10.1016/j.rinp. 2022.106152.
- Waqas H, Farooq U, Liu D, Alghamdi M, Noreen S, Muhammad T. 2022. Numerical investigation of nanofluid flow with gold and silver nanoparticles injected inside a stenotic artery. Mater Design. 223:111130. doi: 10.1016/j.matdes.2022.111130.
- Wu M, Li X, Guo Q, Li J, Xu G, Li G, Wang J, Zhang X. 2021. Magnetic mesoporous silica nanoparticles-aided dual MR/NIRF imaging to identify macrophage enrichment in atherosclerotic plaques. Nanomedicine. 32: 102330. doi: 10.1016/j.nano.2020.102330.
- Xiao Y, Lin J, Zhao Y, Wang X, Lv Q, Li W, Tang R, Fu G. 2024. Plaque-specific adhesive balloons coated with calcium phosphate nanoparticles loaded with rapamycin for atherosclerosis therapy. Adv Funct Materials. 34(24). doi: 10.1002/adfm.202315317.
- Zaman A, Ali N, Kousar N. 2018. Nanoparticles (Cu, TiO2, Al2O3) analysis on unsteady blood flow through an artery with a combination of stenosis and aneurysm. Comp Math Appl. 76(9):2179-2191. doi: 10.1016/j. camwa.2018.08.019.
- Zaman A, Ali N, Sajjad M. 2019. Effects of nanoparticles (Cu, TiO2, Al2O3) on unsteady blood flow through a curved overlapping stenosed channel. Math Comput Simul. 156:279-293. doi: 10.1016/j.matcom.2018.08.012.
- Zhang L, Bhatti MM, Marin M, S. Mekheimer K. 2020. Entropy analysis on the blood flow through anisotropically tapered arteries filled with magnetic zinc-oxide (ZnO) nanoparticles. Entropy. 22(10):1070. doi: 10.3390/ e22101070.
- Zheng J. 2014. Numerical simulation of nanoparticle transportation and deposition in pulmonary vasculature. Michigan: Lehigh University.
- Ziental D, Czarczynska-Goslinska B, Mlynarczyk DT, Glowacka-Sobotta A, Stanisz B, Goslinski T, Sobotta L. 2020. Titanium dioxide nanoparticles: prospects and applications in medicine. Nanomaterials. 10(2):387. doi: 10.3390/nano10020387.